A new specimen of the ornithischian dinosaur *Hesperosaurus mjosi* from the

Upper Jurassic Morrison Formation of Montana, USA, and implications for growth

and size in Morrison stegosaurs

SUSANNAH C. R. MAIDMENT,[1,2]* D. CARY WOODRUFF,[3,4] AND JOHN R. HORNER[5]

[1]Department of Earth Science and Engineering, Imperial College London, South Kensington

Campus, London, SW7 2AZ, United Kingdom;

[2]Current address: School of Environment and Technology, University of Brighton, Lewes Road,

Brighton BN2 4GJ, United Kingdom, s.maidment@brighton.ac.uk;

[3]Great Plains Dinosaur Museum, Malta, Montana, 59538, U. S. A.;

[4]Department of Ecology and Evolutionary Biology, University of Toronto, Toronto, Ontario,

Canada, sauropod4@gmail.com;

[5]Burke Museum of Natural History and Culture, University of Washington, Seattle, Washington,

98195, U.S.A, johnrhorner@mac.com

*Corresponding author

ABSTRACT—Stegosauria is a clade of ornithischian dinosaurs characterized by a bizarre array of dermal armor that extends from the neck to the end of the tail. Two genera of stegosaur are currently recognised from North America: the well-known *Stegosaurus stenops*, and the much rarer *Hesperosaurus mjosi*. A new specimen of *Hesperosaurus mjosi* was discovered in some of the most northerly outcrops of the Upper Jurassic Morrison Formation near Livingston, Montana. The new specimen comprises cranial, vertebral and appendicular material as well as a dermal plate, and the excellent state of preservation of the palate reveals new anatomical information about this region in stegosaurs. Histological examination of the tibia indicates that the individual was not skeletally mature at time of death. Comparison with previously studied *Stegosaurus* and *Hesperosaurus* individuals indicates that *Hesperosaurus mjosi* may have been a smaller genus than *Stegosaurus stenops*. Physiological processes scale with body mass, M, according to the relationship $M^{0.75}$ in extant megaherbivores, thus larger animals are better able to cope with more arid environments where forage is less abundant. Under this scenario, it is possible that *Stegosaurus stenops* and *Hesperosaurus mjosi* were environmentally partitioned, with the larger *S. stenops* occupying more arid environments. Analyses of the temporal overlap and latitudinal range of Morrison stegosaurs would allow this hypothesis to be investigated.

INTRODUCTION

Stegosauria are a clade of thyreophoran 'armored' ornithischian dinosaurs characterized by a bizarre array of hypertrophied dermal armor extending, in two parasagittal rows, from the head to the end of the tail. Stegosaurs are some of the most iconic and easily recognisable dinosaurs, but surprisingly, given their popular status, stegosaurian dinosaur fossils are actually rather rare, and consequently much remains unknown about the paleobiology and paleoecology of the group.

Two stegosaur genera are currently recognised from the Upper Jurassic Morrison Formation of the western U.S.A (Maidment et al., 2008; Carpenter et al., 2001; Carpenter, 2010; Raven and Maidment, in press) However, due to small sample sizes and the fragmentary nature of many specimens, species-level taxonomy is controversial, with some workers considering *Hesperosaurus mjosi* is a species of *Stegosaurus* (Maidment et al., 2008), and some considering that specimens considered by Maidment et al. (2008) as *Stegosaurus stenops* (=*Stegosaurus armatus* therein; ICZN, 2013) belong to more than one species (Carpenter and Galton, 2001; Carpenter, 2010; Galton and Carpenter, 2016).

The vast majority of stegosaur specimens collected and described from the Morrison Formation have been found in Colorado and Utah and, when it is possible to refer them to a genus, are referable to *Stegosaurus stenops* (Maidment et al., 2008; Maidment et al., 2015). A single specimen of *Hesperosaurus mjosi* has been described (Carpenter et al., 2001) and it is from Wyoming. Further specimens of *Hesperosaurus mjosi* are known from Wyoming and

apparently Montana, although all reside in private collections and are thus unavailable for study (SCRM, pers. obs.).

Herein, we describe a new specimen of *Hesperosaurus mjosi* from Montana, from some of the most northerly outcrops of the Morrison Formation. This specimen provides a wealth of new anatomical information about *Hesperosaurus mjosi* because it includes limb bones and skull elements not preserved in the holotype. Additionally, the specimen provides more data on the palate than is known in any other stegosaur. We investigate the osteological maturity of the specimen using bone histology, and discuss implications for growth and size inMorrison Formation stegosaurs.

Institutional Abbreviations—**DMNH**, Denver Museum of Nature and Science, Colorado, U.S.A.; **HMNH**, Hayashibara Museum of Natural History, Okayama, Japan; **MB**, Museum für Naturkunde, Berlin, Germany; **MOR**, Museum of the Rockies, Bozeman, Montana, U.S.A.; **NHMUK**, The Natural History Museum, London, U.K.; **SMA, VFSMA**, Sauriermuseum Aathal, Switzerland; **USNM**, National Museum of Natural History, Smithsonian Institution, Washington D.C., U.S.A.; **ZDM**, Zigong Dinosaur Museum, Sichuan, People's Republic of China.

METHODS

Histologic analysis of the specimen was conducted on the tibia and fibula. An entire transverse section from each element was removed mid-diaphysis. Preparation and execution followed the standard histologic procedures and techniques outlined in Padian and Lamm (2013). All samples were first embedded in a Silmar two-part epoxy resin (SIL95BA-41), and

once cured, slices were cut (~2-4 mm thick) from the block using a Felker 41-AR tile saw. The cut slices were then pre-mount ground on the surface to be glued to the glass slide using 320 and then 600 grit silicon carbide paper. Once the pre-mount grinding was complete, the sample was mounted to a frosted glass slide using a Devcon two-part epoxy glue. Then using a Buehler Ecomet 4 Variable Speed Grinder-Polisher, the thin sections were polished using Buhler silicon carbide paper sequentially from a 60 grit to an 800 grit finish. Final slide thickness depended entirely on optical clarity (in some cases down to ~53 µm). Finished slides were photographed using a Nikon Optiphot-Pol polarizing microscope equipped with a Nikon DS-Fi1 digital camera and compiled with a NIS-Elements BR 3.0 software.

SYSTEMATIC PALAEONTOLOGY

DINOSAURIA Owen, 1842

ORNITHISCHIA Seeley, 1887

THYREOPHORA Nopcsa, 1915 (sensu Norman 1984)

STEGOSAURIA Marsh, 1877

STEGOSAURIDAE Marsh, 1880

HESPEROSAURUS Carpenter et al., 2001

HESPEROSAURUS MJOSI Carpenter et al., 2001

Revised Diagnosis—*Hesperosaurus mjosi* possesses the following combination of plesiomorphic characters and autapomorphies (the latter marked with an '*'): (1) no contact between the lacrimal and prefrontal on the lateral surface of the skull; (2) ventral margin of axis upwardly concave in lateral view*; (3) postzygapophyses not elevated significantly on posterior cervical vertebrae; (4) prezygapophyses join ventrally and face dorsomedially in anterior dorsal vertebrae; (5) dorsal neural arch pedicels not elongated above the neural canal in mid-dorsal vertebrae; (6) dorsal ribs distally expanded; (7) ossified epaxial tendons present; (8) caudal neural spines not bifurcated; (9) dorsal dermal plates longer anteroposteriorly than tall dorsoventrally*.

Holotype—HMNH 001, a nearly complete, disarticulated skull, complete vertebral column, partial left scapula, ilia, ischia, pubes, 10 dermal plates and four tail spines. The specimen was described and figured in Carpenter et al. (2001). A cast of the specimen is housed at the DMNH and is catalogued under the number DMNH 29431. The cast was used for comparative purposes herein.

Referred Specimens—MOR 9728, a partial skeleton including a nearly complete skull, eight cervical vertebrae, one dorsal vertebra, two sacral vertebrae, the right scapulocoracoid and parts of the left element, both humeri, the right tibia, fibula, astragalus and calcaneum, a metatarsal, and a partial dermal plate.

Occurrence—Upper Jurassic Morrison Formation of Wyoming and Montana.

Systematic Remarks—Maidment et al. (2008) diagnosed *Hesperosaurus mjosi* (=*Stegosaurus mjosi* therein) as follows on the basis of a combination of plesiomorphic and autapomorphic characters: *Hesperosaurus mjosi* differs from *S. stenops* by possession of the

following primitive characters: (1) atlas neural arches not fused to the intercentrum in ontogenetically mature individuals; (2) postzygapophyses not elevated significantly on posterior cervical vertebrae; (3) neural arches of dorsal vertebrae not elongated above the neural canal; (4) ossified expaxial tendons present; (5) ribs distally expanded; (6) caudal neural spines not bifurcated; (7) enlargement of the distal end of the pubis. It also has the following autapomorphies: (8) 11 dorsal vertebrae; (9) fourth sacral vertebra not fused to the sacrum; (10) dorsal dermal plates longer anteroposteriorly than tall dorsoventrally.

Additional anatomic information provided by MOR 9728, and a recent description of an almost complete specimen of *Stegosaurus stenops* (Maidment et al., 2015) allows reinvestigation of these features in the light of new data. The atlantal neural arches appear to be fused to the intercentrum in MOR 9728, suggesting that character (1) may be due to individual variation. Maidment et al. (2015) noted that enlargement at the distal end of the pubis (character 7) was variable among specimens and continuous in nature, and it is therefore removed as a diagnostic character of *H. mjosi*. The number of vertebrae fused together to form the sacral rod (character 9) is variable within genera in Stegosauria (Maidment et al., 2008), and may be related to size, ontogenetic stage, or other individual variation. Galton (1982) suggested that it may be sexually dimorphic in *Kentrosaurus.* This character is therefore removed as an autapomorphy for *H. mjosi* herein. Character 8, 11 dorsal vertebrae, is incorrect: there are 13 dorsal vertebrae in DMNH 29431 when the two dorsals that are fused to the sacral rod are taken into account (Maidment et al., 2015).

Preservation of the complete dorsal vertebral column in NHMUK R36730 (*Stegosaurus stenops*) shows that dorsal neural arch pedicel height increases from the most anterior dorsals

to the mid-dorsals, and then decreases again in the posterior dorsals (Maidment et al., 2015).

The lack of elongation of the neural arch pedicels above the neural canal cannot therefore be

used to diagnose *H. mjosi* unless the location on the vertebral column is known (character 3).

However, the anterior dorsals of NHMUK R36730 (*Stegosaurus stenops*) possess

prezygapophyses that are separated from each other and face dorsally. This contrasts with the

condition in *H. mjosi* (DMNH 29431) where the prezygapophyses of anterior dorsals are joined

ventrally and face dorsomedially. This condition is seen in the mid-dorsals of *H. stenops*

(NHMUK R36730; Maidment et al. 2015), which are characterised by elongate neural arch

pedicels. Thus, the combination of prezygapophyses joined ventrally and projecting

dorsomedially and a lack of elongation of the neural arch pedicels allows *H. mjosi* to be

differentiated from *S. stenops*.

MOR 9728 does not offer additional anatomical information on characters (2), (4), (5),

(6) and (10) and these are retained as diagnostic characters. An additional, probably

plesiomorphic characteristic of *H. mjosi* is noted in the well-preserved skull of MOR 9728: the

prefrontal does not extend anterior to the anterior supraorbital, so that it does not contact the

lacrimal. A similar condition is observed in the basal stegosaur *Huayangosaurus*. Furthermore,

the ventral margin of the axis is upwardly concave in MOR 9728 and DMNH 29431, while in

other stegosaurs (*S. stenops*, *Loricatosaurus, Kentrosaurus*) it is flat in ventral view, and this is

interpreted as autapomorphic herein (see the description below for more details about these

features).

GEOLOGICAL SETTING AND DISCOVERY OF THE NEW SPECIMEN

MOR 9728 was discovered at the MOR's O'Hair quarry (formerly known as the Strickland Creek quarry) in 2015 (Fig. 1; T3S R9E). This site has also produced remains of *Diplodocus, Apatosaurus, Camarasaurus* and *Allosaurus* (Cooley and Schmitt, 1998; Whitlock and Harris, 2010 [MOR 592]; Woodruff and Fowler, 2012; Woodruff, unpubl. data). The specimen was found in strata roughly laterally equivalent to those of the upper quarry level, which has previously produced *Diplodocus* and *Allosaurus* remains. The Morrison Formation in the area is not well-exposed, but at the quarry it comprises dull grey and purplish siltstones interbedded with laterally discontinuous fine-grained to conglomeratic sandstones. The uppermost sandstone contains decimeter-scale trough cross-beds and ripple cross lamination in its upper parts (Fig. 2). Morrison channel sandstones in the area have been described as representing anastomosing channels (Cooley and Schmidt, 1998), indicating high rates of aggradation of the floodplain in response to rapid basin subsidence.

With the exception of the dorsal neural arch, the specimen was excavated and removed in a single field jacket (Fig. 3). Along with the stegosaur remains, the jacket also contained a partial femur and dorsal vertebra from a large ornithopod, a caudal vertebra from a large theropod, and an ischium and phalanges from a small ornithopod.

OSTEOLOGICAL DESCRIPTION

The skull is preserved in articulation with the atlas and axis. It is preserved in five separate blocks, numbered 1-5 in the below description, and as shown on Fig. 4. The skull is strongly crushed dorsoventrally.

Skull Roof

The premaxilla is not preserved.

Maxilla—The main part of the maxilla is not preserved; however, the posterior ends of the posterodorsal and posteroventral processes are preserved on the right lateral side of the skull in skull block 2 (Fig. 5). Ventrally, the posteroventral process bears a sharp ridge that projects ventrally and divides the ventral surface into two upwardly concave surfaces (Fig. 5C, D). A process from the ectopterygoid projects anterolaterally and contacts the posteriormost portion of the maxilla (Fig. 5C, D). The anterior process of the jugal projects anteriorly and overlies the posteroventral process of the maxilla ventrolaterally. The posterodorsal process of the maxilla projects posterodorsally to contact the lacrimal and anterior supraorbital (Fig. 5E, F). The two maxillary processes are separated by a narrow gap infilled with matrix, and when the front of the block is in examined, it can be seen that a thin lamina of bone is inset and curves medially from the ventral process to the dorsal process. The matrix-filled gap is interpreted as the antorbital fossa (Fig. 5). An antorbital fossa is also known in *Huayangosaurus* (ZDM T7001; Sereno and Dong, 1992) and the holotype of *Hesperosaurus mjosi* (DNMH 29431; Carpenter et al., 2001), but its presence in *Stegosaurus stenops* has been difficult to ascertain because of the degree of crushing and poor preservation of skull material (USNM 4934; DMNH 2818; NHMUK R36730).

Nasal—Small fragments of both nasals are preserved on skull block 1 (Fig. 6). They are incomplete anteriorly, posteriorly and laterally. A straight, sagittal suture is observed between the elements, and the bone surface lateral to the suture is striated parallel to it. The elements angle ventrally towards the suture. The posteriormost portion of the nasals is preserved on skull block 2 (Fig. 5). They are smooth and flat in dorsal view (Fig. 5A, B). Very subtle, raised ridges indicate the suture with the frontals. The prefrontals overlap the nasals posterolaterally. A posterior process extends posteriorly from the sagittal nasal suture between the frontals (Fig. 5A, B).

Lacrimal—The right lacrimal can be observed on the side of skull block 2 (Fig. 5). Dorsoventral crushing has resulted in apparent anteroventral rotation of the lacrimal, so that it lies obliquely. The lacrimal forms the anterior margin of the orbit. Posterodorsally it is overlain by the anterior supraorbital, while anterodorsally it contacts the posterodorsal process of the maxilla (Fig. 5E, F). Anteroventrally it forms the posterior part of the small gap between the posterodorsal and posteroventral processes of the maxilla, and thus, in its undeformed state, would have formed the posterior margin of the antorbital fossa.

Prefrontal—Both prefrontals are preserved on skull block 2 (Fig. 5) and they presumably continue onto blocks 3 and 4, although the bone surface of these blocks is poorly preserved and sutural contacts are obscured (Fig. 7, 8). The prefrontals are oval elements with the long axis orientated anteroposteriorly. They overlap the nasals and frontals anteriorly and medially on the skull roof (Fig. 5A, B). Laterally the prefrontals are overlain by the anterior supraorbital; sutures with the median supraorbital cannot be seen due to poor preservation of the skull roof in blocks 3 and 4. In contrast to the condition in *Stegosaurus stenops* (USNM 4934; NHMUK

R36730) the prefrontal does not extend further anteriorly than the anterior supraorbital (Fig. 5A, B), and thus there is no visible contact between the prefrontal and lacrimal on the lateral surface of the skull (Fig. 5E, F). This is similar to the condition observed in *Huayangosaurus* (ZDM T7001).

Frontal—The anterior portions of both frontals are present on skull block 2 (Fig. 5; f). Their surfaces are flat and smooth. A process from the nasal extends posteriorly between the frontals. The sagittal suture between the frontals is straight and vertical (Fig. 5A, B). The posterior portion of the frontals is exposed on skull blocks 3 and 4, but the bone surface of these blocks is poorly preserved and highly fractured, and no sutures can be observed (Fig. 7).

Supraorbitals—The anteriormost part of the right anterior supraorbital is preserved in skull block 2 (Fig. 5), and the remains of it and the median and posterior supraorbitals on the right side are preserved in skull block 4 (Fig. 7). The left posterior supraorbital is present in skull block 3 (Fig. 8C, D). The anterior part of the right anterior supraorbital is triangular in dorsal view with an elongate, tapering anterior process that overhangs the lateral side of the skull and is slightly rugose anteriorly (Fig. 5A, B, E, F). The medial surface of the anterior process contacts the prefrontal. Posteriorly, the element flares transversely, retaining contact with the prefrontal anteromedially, and the median superorbital posteromedially (Fig. 7A, B).

The median supraorbital is diamond-shaped and contacts the prefrontal and, more posteriorly, the frontal along its medial surface. Laterally it contacts the anterior supraorbital while posteriorly it contacts the posterior supraorbital (Fig. 7A, B).

The posterior supraorbital is a scute-like element that is ellipsoidal in dorsal view with the long axis anteroposterior (Fig. 7A, B). In lateral view it is roughly triangular with the apex

pointing ventrally (Fig. 7D, E; 8C, D). The posterior supraorbital possesses a small horn-like

projection on its dorsolateral surface that is rugose. Anterodorsally, the posterior supraorbital

contacts the anterior supraorbital and medially it contacts the median supraorbital along an

apparently straight suture (Fig. 7A, B). Posteriorly, the posterior supraorbital overlies the

dorsolateral surface of the postorbital and extends a short distance down the ventral process of

the postorbital (Fig. 7D, E).

Postorbital—Small parts of both postorbitals are preserved on either side, but the right

is better preserved (Fig. 7, 8). The posterior process is elongate, projects posteriorly, and is D-

shaped in cross-section with a flattened dorsal surface and a ventrally rounded ventral surface.

A tapering suture with the squamosal is visible (Fig. 7A, B). The posterior process forms the

lateral margin of the supratemporal fenestra. At the anterolateral corner of the fenestra, a

foramen pierces the internal surface of the postorbital. The medial process of the postorbital

projects medially to contact the frontal, but sutures cannot be seen (Fig. 7A, B). The ventral

process is only partially preserved. It is triangular in cross-section with the apex pointing

medially (Fig. 7D, E). The apex forms an anteroposteriorly thin lamina that projects medially,

and the anterior and posterior surfaces of the posterior process are gently concave.

Jugal—The anterior process of the jugal extends anteriorly to form the ventral margin of

the orbit (Fig. 5, 8). It is well preserved in skull block 3, although the remainder of the bone is

not preserved (Fig. 8). The anterior process is extremely dorsoventrally compressed (Fig. 8C, D).

The ectopterygoid contacts the medial surface of the jugal towards the anterior part of the

orbit (Fig. 8A, B). The jugal laterally overlaps the posteroventral process of the maxilla ventral to

the lacrimal and anterior to the orbit (Fig. 5E, F).

Quadrate—The heads of both quadrates are preserved on skull block 5 (Fig. 9).

Dorsoventral crushing of the skull has resulted in the ventral parts of both quadrates being

rotated anteriorly so that they angle strongly anteroventrally (Fig. 9E-H). The left quadrate is

better preserved than the right. The head of the quadrate is strongly anteroposteriorly

compressed and is transversely broad. The dorsal end of the element is tongue-shaped, being

rounded along its dorsal margin and parallel –sided ventrally, although the ventral portions of

the element are missing (Fig. 9E, F). The dorsal margin of the quadrate articulated with the

squamosal via a deeply concave facet on the ventral surface of the latter, and anteriorly

overlapped the anterior surface of the paroccipital process, to which it now adheres (Fig. 9G,

H). Poor preservation means little further detail can be made out. Neither quadratojugal is

preserved.

Squamosal—Both squamosals are preserved in skull block 5 (Fig. 9). In dorsal view they

are triradiate with an anterior process, a medial process and a short posterior horn-like process

(Fig. 9A, B). The anterior process of the right squamosal can be seen to underlap medially the

posterior process of the postorbital, but the sutures of the medial process with the parietal are

obscured by poor preservation of the skull roof in this region (Fig. 9A, B). Ventrally, the

squamosals bear two concave surfaces separated by an anteroposteriorly-extending lamina.

The surface medial to the lamina is flat to slightly concave and forms the internal lateral and

posterior wall of the supratemporal fenestra. The lateral-most surface is deeply concave and

would have been the articular facet for the head of the quadrate. Although both quadrates are

preserved, they are now dislocated from these facets.

Parietal—The parietal is preserved on skull block 5 (Fig. 9). The parietal is square in dorsal view and forms the medial margins of the supratemporal fenestrae. Dorsally it is flat, as in *Stegosaurus stenops* (USNM 4934; DMNH 2818) and *Huayangosaurus* (ZDM T7001). Distinct breaks in slope separate the dorsal surface from the lateral surfaces inside the supratemporal fenestrae. Sutures with surrounding elements cannot be seen (Fig. 9A, B).

Braincase

The braincase is preserved in skull block 5 (Fig. 9, 10). The supraoccipital is partially obscured by the articulated atlas and axis. It forms the posterior margin of the skull and bears a strong midline ridge extending dorsoventrally from the presumed location of the foramen magnum. The paroccipital processes extend strongly posterolaterally, although this has probably been accentuated by crushing. The paroccipital processes flare distally, and the heads of the quadrates adhere to their anterior surfaces (Fig. 9C, D, 10). Posttemporal foramina are not clear, but the skull is not well preserved in this region.

The occipital condyle is only visible in ventral view due to the articulation of the axis and atlas (Fig. 9C, D, 10). The occipital condyle is small and ventrally convex. The suture between the basioccipital and the basisphenoid cannot be observed, as in other stegosaur specimens (SCRM pers. obs. 2004-2016). The basal tubera arise anterior to the occipital condyle and are ellipsoidal in ventral view with the long axis angled transversely. They comprise two surfaces separated by a ventral ridge. The posterior surface is flat and faces posteroventrally, while the anterior surface is ventrally convex. The basal tubera are separated by a sagittal groove (Fig. 9C, D, 10). Anterior to the basal tubera, the braincase is not well preserved, and details of the

anatomy cannot be determined. However, a small portion of the distal end of the left basipterygoid process is preserved in articulation with the posterior process of the pterygoid on skull block 3. It is rounded in cross-section and flares distally where it articulates with the pterygoid.

The left lateral side of the braincase is better preserved than the right (Fig. 10). Breakages of the braincase, which have subsequently been repaired, roughly correspond to the expected margins of individual braincase elements, and perhaps suggest that the braincase was not fully fused at time of death. The crista prootica, an elongate, caudal process of the prootic that forms a distinct posterodorsally-extending ridge, can be observed in left lateral view (Fig. 10), and beneath it is an oval fossa which represents the combined fenestra ovalis and fenestra pseudorotunda, and the exit of the glossopharangeal, vagus, and accessory nerves (Fig. 10). This fossa is infilled with matrix and thus the crista interfenestralis, which separates the fenestra ovalis and fenestra pseudorotunda (Galton, 1988), cannot be observed. A breakage of the braincase and skull roof probably corresponds to the approximate location of the anterior margin of the prootic. The trigeminal foramen, for the exit of the maxillary and mandibular branches of the trigeminal nerve, is likely located along this breakage, although a distinct foramen cannot be seen (Fig. 10). A breakage ventral to the fossa for the fenestra ovalis and fenestra pseudorotunda may represent the suture between the basioccipital – basisphenoid and the prootic. Foramina for the facial nerve and the internal carotid artery, which are commonly preserved in stegosaur braincases posterior to the trigeminal foramen (SCRM, pers. obs.), are not seen in this specimen, presumably due to poor preservation.

Anterodorsal to the trigeminal foramen lie two deeply excavated fossae in the laterosphenoid which presumably extend into the sella turcica. These fossae are probably for the abducens nerve and pituitary vein (Fig. 10). Anterior to the sella turcica, a dorsoventrally deep, transversely compressed, sagittally extending lamina projects and is broken anteriorly. This presumably represents the cultriform process of the parasphenoid (Fig. 9E, F). The orbitosphenoids are not preserved in this specimen, and further details of the anatomy of the braincase cannot be seen due to poor preservation.

Palate

Vomer—The vomers are preserved in skull blocks 2 and 3 (Fig. 5, 8). Extending anteriorly from the pterygoid, they constitute two vertical, transversely thin sheets of bone that are joined ventrally posteriorly but appear to separate anteriorly, although are incomplete ventrally in this region (Fig. 5C, D). They extend between the palatines and appear to project forward to contact the premaxilla, although this region is poorly preserved. The sutural boundary between the vomers and the pterygoid cannot be seen.

Palatine—Both palatines are preserved on skull blocks 2 and 3 (Fig. 5, 8), although the left is the most complete. The palatines are dorsoventrally thin, triangular sheets of bone (Fig. 5C, D) that extend anteriorly from the pterygoid (Fig. 8A, B). The sutural boundary between the palatines and pterygoid is not clear. The palatines project anteriorly to just anterior to the maxilla-jugal suture on the lateral side of the skull. They are shallowly upwardly concave. The ecotopterygoid appears to overlap the palatine ventrally in a broad, tongue-like process (Fig. 5C, D).

Ectopterygoid—Both ectopterygoids are preserved. The right is preserved in skull block 2 (Fig. 5C, D), while the left is preserved in skull block 3 (Fig. 8). The ectopterygoid appears to contact the palatine and pterygoid medially, and the jugal and maxilla laterally (Fig. 5C, D; 8). Anteriorly, the medial end of the ectopterygoid laps ventrally onto the ventral surface of the palatine about half way along the length of the latter. The area of contact with the palatine is dorsoventrally compressed. Lateral to the palatine articulation, the ectopterygoid turns ventrally and projects posteriorly to contact the anterior process of the pterygoid, which it overlaps medially. Anterior of its contact with the pterygoid, the element rises dorsally and expands anteroposteriorly to form a broad, fan-shaped process that contacts the ventromedial surface of the anterior process of the jugal immediately below the anterior part of the orbit. It also sends out an anteroposteriorly thin anterolateral process to contact the posteroventral process of the maxilla (Fig. 5C, D).

Pterygoid—Part of the left pterygoid is preserved in skull block 3 (Fig. 8). It comprises a dorsoventrally compressed anterior process that projects anterolaterally to a level about midway along the orbit, and tapers to a point (Fig. 8A, B). The ectypterygoid overlaps this process on its medial surface. Sutures with the vomers and palatines cannot be seen. The posterior process of the pterygoid is dorsoventrally deep relative to the anterior process, transversely compressed, and rounded along its posterior margin (Fig. 8A, B). A small portion of the pterygoid process of the quadrate is preserved adhering to its posteromedial surface (Fig. 8A, B), and dorsal to this, the left basipterygoid process articulates with the posterior process of the pterygoid near its divergence point from the main body of the pterygoid.

Axial Skeleton

Measurements of the axial skeleton can be found in Table 1.

Atlas—The atlas and axis are associated with the skull and consequently some details of their anatomy are obscured (Fig. 9). The right lateral side of the atlas is best preserved (Fig. 9G, H); ventrally it is eroded and the left lateral side is fractured (Fig. 9C, D). The atlantal intercentrum is present as a ring-like element located between the braincase and the axis, and few details of its anatomy are preserved. In right lateral view, the lateral surface of the intercentrum bears a rugosity immediately below a shallow, horizontal, anteroposteriorly extending groove that marks the suture between the atlas neural arch and intercentrum. In lateral view, the atlas neural arch is inverted comma-shaped, tapering distally as it extends posterodorsally (Fig. 9G, H). Carpenter et al. (2001) suggested that the atlas neural arches were not fused to the intercentrum in *S. mjosi*; however, fusion of the atlas neural arches is variable among specimens of *S. stenops* (Gilmore 1914) and it appears that this is also the case in *S. mjosi*.

Axis—The axis is well-preserved although crushed dorsoventrally and closely associated with the atlas and skull, so the odontoid process cannot be observed. In ventral view, the centrum is spool-shaped with constricted lateral margins and flared anterior and posterior ends (Fig. 9C, D). The ventral surface is saddle-shaped, being concave anteroposteriorly but transversely convex. This contrasts with the condition in *Stegosaurus stenops* (NHMUK R36730; Maidment et al., 2015), *Loricatosaurus* (NHMUK R3167; Galton, 1985) and *Kentrosaurus* (MB R.4779), but is similar to the condition in the holotype of *Hesperosaurus mjosi* (DMNH 29431; Carpenter et al., 2001). Two ridges extend from the posterior margin of the ventral centrum

either side of the midline and project anteriorly before merging with the ventral surface at about midlength (Fig. 9C, D). A subtle central ridge is also present, as in other stegosaurs in which the axis is known (*S. stenops*, NHMUK R36730, Maidment et al., 2015; *Kentrosaurus,* MB R4779; *Loricatosaurus,* NHMUK R3167, Galton, 1985). The right lateral side of the centrum is better preserved than the left lateral side. The right parapophysis is prominent and projects laterally from the lateral surface of the centrum behind the anterior margin of the articular facet (Fig. 9C, D). It is a dorsoventrally compressed flange and its lateral projection has probably been accentuated by crushing. The right diapophysis projects laterally from a location posterior to the parapophysis and a horizontal, posteriorly-extending groove separates the two. The diapophysis is dorsoventrally compressed, rectangular in dorsal view with the long axis trending anteroposterior, slightly convex on the dorsal surface and slightly concave on the ventral surface. The posterior articular facet of the centrum is ellipsoidal in posterior view with the long axis trending transversely and is shallowly concave.

In lateral view, the neural arch is low and rectangular with the long axis trending anteroposterior, although it is dorsoventrally crushed (Fig. 9E, F). The neural arch extends posteriorly so that it greatly overhangs the posterior articular facet. The suture with the axis centrum cannot be seen, but dorsal to the presumed location of the suture, the surface of the neural arch is strongly convex and rugose. From this surface, a transversely compressed flange, the neural spine, extends dorsally and has a flattened, slightly expanded top. Postzygapophyses extend posteriorly from the convex surface of the neural arch and their articular surfaces are angled ventrolaterally. In posterior view the postzygapophyses are separated by a broad, upwardly convex arch. Dorsal to the postzygapophyses, two ridges, the epipophyses, arise from

the posterior margin of the neural arch and extend a short distance anteriorly. The posterior

end of the neural spine ends in a bluntly broken process that extends posteriorly between and

dorsal to the epipophyses.

Postaxial Cervical Vertebrae

The remaining cervical vertebrae were not articulated so their order is unknown; they

are labelled 1-6 here for clarity and for comparison with Figures 11-13. Most are represented by

centra alone, although isolated neural arches are also preserved. Minimally there are 6

postaxial cervical vertebrae although as many as 9 could be represented in the preserved

material.

Cervical 1—Only the centrum is preserved (Fig. 11). The centrum is longer

anteroposteriorly than it is wide transversely, similar to the condition in other stegosaurs

except for *Dacentrurus armatus* (NHMUK OR 46013), in which the reverse is true. It is spool-

shaped in ventral view with a saddle-shaped ventral surface. Two prominent ridges extend from

the anterior margin along the ventral surface either side of the midline, merging in the middle

of the centrum (Fig. 11C). The ventral surface of the posterior part of the centrum is rugose and

striated. The anterior articular facet is roughly D-shaped with a flattened dorsal margin. It is

wider transversely than it is high dorsoventrally, and it is shallowly concave. In lateral view,

parapophyses extend from just posterior to the anterior articular facet (Fig. 11). They are

rectangular in dorsal view (Fig. 11B), dorsoventrally compressed, and expand into ellipsoidal

articular surfaces for the ribs distally (Fig. 11E). A horizontal ridge extends from the posterior

margin of the parapophyses a short distance posteriorly. The posterior articular facet is

distorted and fragmentary, but appears to have been concave. The dorsal margin of the centrum is not well enough preserved to determine whether the neural arch was fused and has broken, or whether it remained unfused.

Cervical 2—The centrum and partial neural arch are preserved (Fig. 12), and the two appear to have been fused, although the suture between them is clear posteriorly where the elements are complete. The centrum is dorsoventrally crushed. The centrum is morphologically similar to that described above although the ventral ridges extending from the anterior surface have joined to become a single, transversely broad ridge. The neural canal is ellipsoidal with the long axis trending transversely.

The neural arch preserves both postzygapophyses, the neural spine, and a partial left diapophysis. Prezygapophyses and the anterior portion of the neural arch are not preserved. The postzygapophyses extend posteriorly and slightly dorsally well beyond the posterior articular facet of the centrum (Fig. 12E, F), a feature considered a synapomorphy of *Stegosaurus* by Maidment et al. (2008). They are tongue-shaped in dorsal view and separated by a broad, v-shaped notch (Fig. 12B). The articular surfaces are tear-drop shaped with the apex pointing anteriorly, and the facets face ventrolaterally. A ridge extends from the dorsolateral margin of the postzygopophyseal facet anteroventrally onto the lateral surface of neural arch, projecting forward to form the posterior surface of the diapophysis. This is equivalent to the postzygodiapophyseal lamina of sauropods (PODL; Wilson, 1999; Fig. 12F). Posterior to this ridge is a shallow fossa that extends to the posterior margin of the neural arch. In posterior view, a deep, postspinal fossa is present between the postzygapophyses (Fig. 12D), and at the base of the arch, lateral to the neural canal, a small but deep, matrix-filled fossa is present on

either side. The short, rectangular neural spine arises immediately anterior to the v-shaped notch formed between the postzygapophyses, and projects dorsally (Fig. 12E, F). It has a slightly transversely expanded top. From the posterior margin of the neural spine, ridges extend a short distance down the postzygapophyses (the spinopostzygopophyseal lamina of sauropods; SPOL; Wilson, 1999; Fig. 12B). In dorsal view, the preserved left diapophysis is rectangular with the long axis trending anteroposteriorly (Fig. 12F). It is expanded distally and the articular facet is triangular, with the apex extending anteriorly. By comparison with the cervical vertebrae of NHMUK R36730 (*Stegosaurus stenops;* Maidment et al., 2015), this vertebra is cervical vertebra four, as it does not possess epipophyses but has an elongate v-shaped notch between the postzygapophyses.

Cervicals 3-6—Only centra are preserved in cervicals 3-6, and they are similar in morphology to each other and to those of cervicals 1 and 2. Both anterior and posterior articular facets are ellipsoid in shape with the long axis trending transversely. The posterior facet appears to be larger than the anterior facet, and is more deeply concave. The ventral rugosity extending from the anterior facet posteriorly is still present. Parapophyses are present as dorsoventrally compressed flanges extending from a location just posterior to the anterior articular facet.

Cervical Neural Arches—Three cervical neural arches are preserved separately from the centra. One is isolated and less complete, while two more complete neural arches are associated with one another and their respective pre- and postzygapophyses are preserved in articulation.

The neural arches are slightly larger and more robust than that described for cervical 2, suggesting that they are more posterior cervicals. The more anterior of the neural arches preserves the right diapophysis and prezygapophysis, and both postzygapophyses (Fig. 13). The neural spine is broken off at its base and not preserved. The neural arches are not complete ventrally, so it is not possible to determine whether they were fused and subsequently broken off, or whether they were not fused at time of death. The right diapophysis is lobate in dorsal view, with parallel anterior and posterior margins and a smoothly curved distal tip (Fig. 13B). It is dorsoventrally compressed, bears a shallow concavity on its dorsal surface, and ventrally bears a prominent ridge extending along its length. Such a ridge is not observed on the diapophyses of NHMUK R36730, *Stegosaurus stenops* (Maidment et al., 2015). The articular surface is angled ventrolaterally, is roughly circular in outline, and is concave. The right prezygapophysis is supported on the base of the diapophysis and arises from it (Fig. 13). The articular surface is ellipsoidal in outline with the long axis anteroposterior, and the facet faces dorsomedially. The facet merges gently into a horizontally orientated intraprezygapophyseal shelf which is flat anteriorly but slightly upwardly concave posteriorly (Fig. 13B). From the center of the intraprezygapophyseal shelf a sharp, prominent ridge arises and projects posterodorsally to the base of the neural spine, which is broken. The postzygapophyses project posterolaterally from the base of the broken neural spine, are tongue-shaped, and are separated by a broad U-shaped notch (Fig. 13B). In dorsal view, a rugose ridge extends down each postzygapophysis, merging about half way along their length (Fig. 13B). While a ridge is observed in this location up to cervical four in NHMUK R36730 (*Stegosaurus stenops*), it is not observed in subsequent vertebrae (Maidment et al., 2015). Between the postzygapophyses is a

shallow postspinal fossa. A postspinal fossa is only present in the most anterior cervicals of

NHMUK R36730, *Stegosaurus stenops* (Maidment et al., 2015). The articular surfaces of the

postzygapophyses are angled ventrolaterally and are round in outline, being broader

transversely than they are on the neural arch of cervical 2. A very prominent ridge is continuous

with the ventromedial margin of the articular surface, and extends ventrally along the length of

the postzygapophysis, terminating where the neural arch is broken at its base. The region

between the ventral ridges is roofed by a horizontal lamina which is gently concave ventrally,

forms the base of the postspinal fossa, and the anterior surface of the U-shaped notch between

the postzygapophyses (Fig. 13B). In ventral view, the top of the neural canal is visible and is

smoothly concave. A second neural arch is preserved in articulation with the one described

above, and an isolated neural arch is also present. They are morphologically identical to that

described above.

Cervical Ribs

Three cervical ribs are preserved. By comparison with those of NHMUK R36730 they are

probably left cervical rib six, right cervical rib 8, and left cervical rib 12 or 13.

The capitulum and tuberculum of left cervical rib six (Fig. 14A, B) are separated from

each other by a shallow concavity whose surface is broken anteriorly. The rib is transversely

compressed with a concave medial surface. The capitulum is anteroposteriorly broader than

the tuberculum is dorsoventrally tall, but the tuberculum is longer than the capitulum. The

articular surfaces of both processes are roughly round in outline, and the capitular surface is

larger than the tubercular surface. The rib shaft is curved dorsally along its length, and tapers distally. A prominent ridge extends down its lateral surface.

Cervical rib eight is incomplete distally (Fig. 14C, D). The tuberculum and capitulum are separated by a broad, U-shaped surface and project at 90 degrees from one another. The tuberculum is longer than the capitulum. Both processes are rectangular in lateral view with blunt ends. The articular facet of the tuberculum is roughly rectangular with the long axis dorsoventral, while that of the capitulum is ellipsoidal with the long axis anteroposterior. The shaft tapers distally and a prominent but crushed ridge is present on the lateral surface. The medial surface is concave.

Cervical rib 12 is completely preserved (Fig. 14E, F). The capitulum and tuberculum are separated by a broad U-shaped notch and they project at an angle of roughly 70 degrees to each other. The tuberculum is longer than the capitulum, and is about half the total length of the rib. It is rectangular in lateral view with a narrow, rectangular articular surface. A ridge arises close to its base and extends posteriorly to the end of the shaft of the rib. The capitulum is rectangular in lateral view but the posterior and dorsal margins merge smoothly into one another. It is transversely compressed but the flared slightly at the articular facet, which is ellipsoidal with the long axis anteroposterior. The shaft of the rib tapers distally, projects posteriorly, and curves slightly ventrally at its distal end. The medial surface of the rib is slightly concave.

Dorsal Vertebra

A single neural arch of a dorsal vertebra was found associated with the specimen (Fig. 15). The neural arch is small and complete ventrally, and appears to have been unfused to its respective centrum at time of death, judging by the completeness of the fluted, sinuous articular surface. In anterior view, the neural canal is oval, and the prezygapophyses project anteriorly directly from the top of the neural canal, so that the neural arch pedicels are not elongated dorsally (Fig. 15A). The neural arch pedicles are not strongly elongated above the neural canal in the most anterior dorsals of *Stegosaurus* (NHMUK R36730, Maidment et al., 2015) or *Hesperosaurus* (DMNH 29431, Carpenter et al., 2001), and the preservation of several cervical vertebrae in this specimen suggests that this may be an anterior dorsal neural arch. The prezygapophyses are lobate in shape and their articular surfaces are joined ventrally to form a single concave articular surface with no intraprezygapophyseal shelf (Fig. 15A, E). The articular surfaces are angled dorsomedially. In contrast, the prezygapophyses of the most anterior dorsals in *Stegosaurus stenops* are not joined ventrally, and the articular surfaces angle strongly dorsally (NHMUK R36730, Maidment et al., 2015). However, in *Hesperosaurus mjosi* (DMNH 29431, Carpenter et al., 2001) and *Huayangosaurus taibaii* (ZDM T7001; Zhou et al., 1984) the prezygapophyses of the most anterior dorsals are joined ventrally and angle dorsomedially, as in MOR 9728. Anteriorly, a shallow, subtle ridge extends from the anterior margin of the prezygapophyses where they meet on the midline down a posteroventrally inclined surface to the top of the neural canal. Prominent ridges extend from the dorsal tips of the prezygapophyses to the anterolateral margins of the neural canal (Fig. 15A). The posterior margins of the articular surfaces of the prezygapophyses form a lamina that extends along the anterior surface of each diapophysis (the prezygodiapophyseal lamina of sauropods, PRDL,

Wilson, 1999; Fig. 15B, C). Immediately posterior to the joined articular surfaces of the

prezygapophyses there is a midline concavity backed by a vertical sheet of bone, which is

fractured in this specimen (Fig. 15A). The vertical sheet of bone posterior to the

prezygapophyses is also observed in NHMUK R36730, *Stegosaurus stenops* (Maidment et al.,

2015), but is absent in *Huayangosaurus* (ZDM T7001; Zhou et al., 1984). The diapophyses

diverge from this sheet of bone at an angle of approximate 50 degrees to the horizontal (Fig.

15A, D). Both diapophyses are broken distally. A prominent ridge extends ventrally down the

diapophyses and onto the neural arch, diverging around the parapophysis and forming its

margins (the paradiapophyseal lamina of sauropods, PPDL, Wilson, 1999), and then continuing

to the anterolateral corner of the neural arch (the anterior centrodiapophyseal lamina, ACDL,

Wilson, 1999). This lamina and that extending ventrally from the prezygapophysis border a

shallowly concave fossa on the lateral surface of the neural arch anterior to the parapophysis.

The parapophysis is poorly preserved on both sides but is present at the base of the

diapophysis and is ellipsoidal in shape with the long axis dorsoventral. It is strongly concave,

although this may have been accentuated by crushing (Fig. 15C). In posterior view, the

posterior margins of the diapophyses are shallowly concave (Fig. 15D). The dorsally and

posteriorly incomplete neural spine arises from the vertical sheet backing the prezygapophyseal

fossa at the base of the diapophyses (Fig. 15A, D). It extends vertically but due to poor

preservation, few other features of its anatomy can be described. The PODL extends posteriorly

from the diapophyses to the postzygapophyses (Fig. 15E). The articular surfaces of the

postzygapophyses angle ventrolaterally and are separated from each other by a midline groove

(Fig. 15D). In posterior view, the SPOL extends ventrally to the dorsal surface of the

postzygapophyses, which form a triangular wedge with the apex pointing ventrally. Ventral to the postzygapophyses and dorsal to the neural canal, the neural arch is flat.

Dorsal Rib

A small fragment of dorsal rib is present. It is L-shaped, being convex on the presumably anterior surface. The presumed posterior surface is divided into two by a distinct ridge: a posteriorly facing surface and a dorsally facing surface. The element is curved along its length and presumably represents part of the proximal portion of the rib distal to the articular facets.

Sacral Vertebrae

A complete sacral centrum is fused to a second partial sacral centrum (Fig. 16). It is not possible to determine which sacrals these are. The complete centrum is spool-shaped in ventral view, being strongly constricted medially at its center (Fig. 16B). Ventrally it is slightly crushed but no obvious keel is present. The anterior articular facet is much broader transversely than it is tall dorsoventrally and is flat (Fig. 16C). The broad anterior width is due to parapophyses that are drawn out laterally from immediately posterior to the anterior articular facet (Fig. 16C). The parapophyses are triangular in anterior view with the apex pointing laterally and rectangular in dorsal view with the long axis orientated anteroposterior. The neural canal incises strongly into the top of the articular facet (Fig. 16A, C). In dorsal view, the centrum bears an anteroposterior U-shaped groove for the neural canal that is deeply incised, but is restricted by a saddle where the two fused sacrals meet (Fig. 16A). The neurocentral suture is fluted and its degree of completeness indicates that the neural arch was not fused to the centrum at time of death. In

lateral view, posterior to the parapophysis, a horizontal, sharp ridge extends posteriorly, and a deep fossa is present above this ridge, bounded dorsally by the open neurocentral suture (Fig. 16D). Irregularly positioned nutrient foramina are present on the ventrolateral surfaces of the centrum. The second fused centrum is incomplete but morphologically consistent with that described above.

Appendicular Skeleton

Measurements of the appendicular skeleton can be found in Table 2.

Scapulocoracoid—The right scapula is fused to the very incomplete coracoid, and the suture between the two cannot be observed, although both are damaged in this region (Fig. 17). Scapulocoracoid fusion varies between specimens in *Stegosaurus stenops* (Gilmore, 1914) and in *Kentrosaurus* (Maidment et al., 2015). The scapula comprises a proximal plate with a rectangular acromial process, which makes a 90 degree angle with the dorsal surface of an elongate, roughly parallel-sided blade, as in specimens of *Stegosaurus* (NHMUK R36730; Gilmore, 1914; Maidment et al., 2015; Fig. 17A, B). The acromial process makes an angle of greater than 90 degrees with the shaft in *Huayangosaurus* (ZDM T7001; Zhou et al., 1984). In lateral view a prominent ridge extends dorsoventrally from the top of the posterior part of the lateral surface of the acromial process towards the ridge along the middle of the blade, and corresponds to the attachment area for the m. deltoideus clavicularis (Maidment and Barrett, 2012; Fig. 17A). The surface of the proximal plate is dorsoventrally and anteroposteriorly concave. In medial view, an embayment into the otherwise smooth medial surface of the proximal plate along its anterior margin indicates the location of the coracoid foramen (Fig.

17B). The glenoid is posteriorly curved in lateral view and oval in outline and deeply concave in anterior view (Fig. 17A, C). The ventral margin of the glenoid extends to a level ventral to the ventral margin of the blade, and on its lateral surface it possesses a rugose muscle scar for the m. triceps longus (Maidment and Barrett, 2012). Medially, another roughened area is present, and the ventral margin is consequently transversely flat (Fig. 17C). The scapula blade is parallel-sided along most of its length, flaring ventrally slightly at its distal end. A very prominent ridge, the area of attachment of the m. deltoideus scapularis (Maidment and Barrett, 2012), divides the lateral surface of the scapula blade into a dorsolaterally-facing surface and a ventrolaterally-facing surface, and is located about one third of the way from the dorsal margin of the blade (Fig. 17A). The ridge extends posteriorly along the blade, decreasing in height, until it merges with the blade about half way along the blade's length. The ventrodistal corner of the scapula blade is gently curved, while the dorsodistal corner is sharper, and slightly damaged. The blade is laterally convex along its length, presumably to curve around the rib cage (Fig. 17C, D).

Very little of the coracoid is preserved. A small portion of the glenoid articulation indicates continuation of the smooth, concave articular surface. In medial view, the embayment in the medial scapula continues onto the coracoid, where it presumably would have formed the coracoid notch, but is broken anteriorly.

A portion of the left scapulocoracoid is preserved proximal to the glenoid. Once again, the coracoid and scapula are fused and there is no clear suture between the two. The glenoid forms an upwardly concave, ellipsoidal cup morphologically consistent with the better preserved right element.

Humerus—The left humerus is rather fragmentary and poorly preserved (Fig. 18). The deltopectoral crest is crushed so that it projects in the anterior plane (Fig. 18A, D). The posterior part of the shaft is fragmentary, and the distal condyles have been slightly sheared obliquely (Fig. 18E). In anterior view the humerus is dumb-bell shaped in outline (Fig. 18A). The anterior surface is poorly preserved for most of the length of the element. The anteromedial surface of the deltopectoral crest now faces medially, as a result of crushing, but is smooth and slightly dorsoventrally convex. Anteriorly, there is a shallow concavity between the distal condyles. A well-developed, triangular supinator ridge extends laterally from just dorsal to the distal condyles (Fig. 18A). The deltopectoral crest is roughly triangular in lateral view with a smoothly curved apex that points anteriorly (Fig. 18B). The lateral surface of the deltopectoral crest is strongly rugose across about half its width extending posteriorly from the apex. Posteriorly the shaft of the humerus is badly damaged, but the head extends posteriorly from the dorsal margin (Fig. 18C). It is broken along its lateral edge, but the ventral, lateral and dorsal surfaces merge into one another to form a gently rounded surface. The head is dorsoventrally and transversely convex and pitted. The distal condyles are separated by an irregular groove that has probably been accentuated by crushing. In ventral view, the outline of the distal condyles is dumb-bell shaped (Fig. 18E). Each condyle is smoothly convex both mediolaterally and anteroposteriorly, and the articular surfaces project further onto the anterior surface of the humerus than they do onto the posterior surface. The condyles are separated by a saddle-shaped depression.

The right humerus is present but poorly preserved, and is in at least four pieces. It is crushed, but appears morphologically consistent with the left humerus.

Tibia, Fibula, Astragalus and Calcaneum—The right tibia, fibula, astragalus and calcaneum are well preserved and fused together into a single element (Fig. 19). In anterior view the tibia has a straight shaft with transversely expanded distal and proximal ends. Proximally, the cnemial crest is represented by an inverted tear-drop shaped rugose area that has been flattened by crushing (Fig. 19A, C). The apex of the tear-drop extends about one-quarter of the way down the shaft of the tibia, before merging with the shaft. The anterior surface of the tibial shaft is flat with distinct medial and lateral ridges, so that in cross-section the shaft is roughly D-shaped. The distal portion of the tibia is crushed anteriorly and consequently is transversely and dorsoventrally concave. The distal end of the fibula is fused to the lateral malleolus of the tibia and can be distinguished because it is slightly raised relative to the surface of the tibia. In lateral view the proximal end extends posteriorly while the cnemial crest is flattened, and overhangs the lateral surface. The shaft is flattened, as it is in anterior view. In posterior view the proximal end is expanded both transversely and posteriorly and it bears a ridge that is directed posterolaterally and extends ventrally about one quarter of the way down the shaft (Fig. 19B). This ridge has probably been accentuated by crushing. A rugose muscle scar is present on the posterior surface medial to the ridge. The posterior surface of the shaft is convex with a narrow, flattened surface. The medial malleolus bears a ridge in posterior view that extends to the distal end, so that in cross-section the medial malleolus is triangular with the apex pointing posteriorly (Fig. 19D). The lateral malleolus is gently dorsoventrally concave. The proximal end of the tibia is roughly ellipsoidal with the long axis trending transversely. The lateral process, for the articulation with the fibula, projects medially as a thin flange that is triangular in proximal view (Fig. 19C).

The astragalus appears to be fused to the distal end of the tibia (Fig. 19A, D), as indicated by a subtle groove extending transversely across the anterior surface of the distal end. The astragalus is roughly rectangular in distal view with the long axis trending transversely; its surface is distally flattened and slightly crushed. In posterior view the astragalus is gently convex and the suture with the tibia cannot be observed.

The fibula is a gracile element that is expanded anteroposteriorly at its proximal end and transversely at its distal end. The proximal end is slightly crushed so that it is c-shaped in proximal view, with the concave side wrapping around the lateral process of the proximal end of the tibia (Fig. 10C). The fibula shaft is D-shaped in cross-section, being flat medially and rounded laterally. Distally, the fibula is firmly fused to the tibia and the distal end is flat transversely in anterior view. The calcaneum appears to be fused anterodistally to the fibula (Fig. 19A, D). The calcaneum has a roughly circular outline in anterior view. Its anterior surface is somewhat crushed and a groove extends across this surface, which is probably due to damage. Distally, the calcaneum expands distal to the surface of the astragalus, but again this is likely accentuated by crushing. The sutures between the fibula, calcaneum and astragalus are largely obscured, with only shallow grooves indicating the margins of each element.

Dermal Armor

The partial dorsal plate is very thin and fragile and preserved on a block of sandstone (Fig. 20). The base of the plate is fractured and broken and little of it remains. The plate is incomplete along most of its margins, except for one anterior/posterior margin, where fingers of bone can be seen thinning into the sandstone block on which the plate is preserved. The

lateral/medial surface of the middle of the plate is well preserved and a single blood vessel pit

extends dorsally, branching into two just dorsal to the base. Both pits then continue dorsally,

extending parallel to each other. The dimensions or relative proportions of the plate cannot be

obtained from this specimen.

HISTOLOGICAL DESCRIPTION

Histologic sampling on the tibia and fibula was conducted to obtain the life history

information of the animal. Due to the mineralogy associated with preservation of the specimen,

the initial thin sections were very dark and had to be ground further for optical clarity (initially

~220 μm down to ~53 μm). Tissue comparisons were made with both the thicker and thinner

scans. Histological descriptions follow those established by Francillon-Vieillot et al. (1990), de

Ricqlès et al. (1991), Castanet et al. (1992), Huttenlocker et al. (2013), and Woodward and Lee

(2013).

In the tibia, the majority of the inner to mid cortex (approximately two-thirds), consists

of a highly remodeled zone predominantly comprising three to four generations of secondary

osteons (determined via overlapping or cross-cutting relationships; Fig. 21). This remodeled

zone is not identified as Haversian bone (*sensu* Huttenlocker et al., 2013) because interstitial

tissue can still be infrequently observed, but due to the degree of remodeling, the predominant

vascular canal orientation in this zone cannot be determined. Progressing to the outer cortex,

the number of generations of secondary osteons decreases (down to a maximum of two

generations), and more of the primary fibrolamellar tissue is visible. While the optical issues

previously mentioned interfere with tracts of this region, in some areas this primary tissue appears to consist of infrequent longitudinal canals. In the outermost regions of the cortex, vascularity appears to decrease, with fewer and fewer longitudinal canals observed, although primary osteons and longitudinal vascular canals can still be observed, and single generations of secondary osteons appear sporadically distributed. Conversely, in examining the fibula thin section, almost the entirety of the cortex is composed of Haversian bone (see Supplemental Information). This emphasizes how examination of the histology of different elements from the same specimen can result in differing life history interpretations (Horner et al., 1999; Woodward et al. 2014).

The generally low degree of vascularity observed within the cortex of MOR 9728 would seem to indicate that stegosaurs had a slower rate of bone growth compared to that of other dinosaurian taxa (following Amprino's rule; Amprino, 1947; Horner and Padian, 2004; Woodward et al., 2015), a conclusion also reached by Redelstorff and Sander (2009) and Hyashi et al. (2009). However, because the inner cortex of MOR 9728 is remodeled, it is possible that the low vascularity observed in the outer cortex is due to slowing growth as the animal approached asymptotic size. Throughout the cortex of the tibia of MOR 9728, Lines of Arrested Growth (LAGs) are observed, yet the aforementioned optical issues and the degree of remodeling result in difficultly in tracing the full extent of these LAGs. Within the cortex we recognize 15 lines to line segments which we interpret as being LAGs. Thus we would hypothesize that MOR 9728 was a minimum of 15 years at the age of death. While decreasing vascularity and the presence of secondary osteons in the outer cortex suggests maturing tissues and a decrease in osteogenesis, an External Fundamental System (EFS), the histologic indicator

of skeletal growth cessation (Huttenlocker et al., 2013; Woodward and Lee; 2013), is not present. While the majority of the LAG record in MOR 9728 is restricted to the outermost cortex, the spacing, vascularity, and presence of primary and secondary osteons amongst these outermost LAGs is not consistent with the microanatomy indicative of an EFS. Again, based on the rates of remodeling and decreasing vascularity in both the tibia and fibula, we hypothesize that MOR 9728 is nearing or close to skeletal maturity, but has not yet reached that threshold.

DISCUSSION

Implications for Ontogeny and Size

The microanatomy within the cortex and lack of an EFS indicates that growth in MOR 9728 was slowing, but the animal had not reached skeletal maturity at time of death. Redelstorff and Sander (2009) examined the long bone histology of three other specimens of *Hesperosaurus mjosi* (SMA0092; SMA0018; VFSMA001) held in a private collection. Although different long bone elements were sampled (humeri, femora, and tibiae), which makes direct comparison complicated, in SMA0092 (humerus length = 403 mm) and VFSMA001 (humerus length = 438 mm), Redelstorff and Sander (2009) observed a decrease in vascularization towards the outer cortex, but no EFS, indicating that growth slowed but had not stopped prior to death. In SMA0018 (humerus length = 545 mm), an incipient EFS was observed, indicating the specimen reached skeletal maturity before death.

Redelstorff and Sander (2009) and Hayashi et al. (2009) histologically sampled the long

bones of two specimens referable to *Stegosaurus stenops*, NHMUK R36730 (SMA RCR0603 of

that study) and DMNH 2818 respectively. NHMUK R36730 (humerus length = 435 mm) did not

show a decrease in vascularity outwards, and woven bone dominated throughout, indicating

growth had not slowed at time of death. DMNH 2818 does not preserve a humerus, but based

on femoral length (1048 mm) is the largest stegosaur specimen so far histologically sampled. It

possesses an EFS, indicating cessation of growth.

SMA0092 and VFSMA001 appear to be at more comparable histologic stages to MOR

9728 than any of these specimens are to the sampled *S. stenops*. With a humerus length of 390

mm, MOR 9728 is also comparable in size to these specimens, with only a minor degree of

intraspecific size variation indicated (10% of the length of the humerus). Interestingly,

Redelstorff and Sander (2009) were only able to observe five LAGs in SMA0092 and three LAGs

in VFSMA001. This LAG count discrepancy between the three specimens does not necessarily

indicate some sort of extreme skeletal plasticity (Sander and Klein, 2005), but instead probably

represents incomplete records due to the degree of remodeling. Redelstorff and Sander (2009)

noted that the degree of remodeling in SMA0092 and VFSMA001 obscured LAGs, and perhaps

the "high" LAG count in MOR 9728 could indicate that some of the observed LAGs are not

proper annual indicators. Instead, they may represent double or triple LAGs (Huttenlocker et

al., 2013; Woodward and Lee; 2013; however Hayashi et al. [2009] noted 12 LAGs in an

indeterminate Morrison Formation stegosaur, DMNH 21068).

Intruigingly, NHMUK R36730, *S. stenops*, was identified by Redelstorff and Sander (2009)

as the histologically youngest specimen in their study, despite possessing a humerus the same

length or longer than the more histologically mature specimens of *H. mjosi.* Furthermore, the fully skeletally mature individual of *H. mjosi* (SMA0018) has a femur 70 mm shorter than that of the fully skeletally mature individual of *S. stenops* (DMNH 2818; SCRM pers. obs. 2005). Based on this admittedly limited sample, the available data suggest that *Hesperosaurus mjosi* might have been a smaller genus than *Stegosaurus stenops*. This size difference could have occurred within the same longevity intervals, or perhaps these two genera had significantly differing growth rates. Further histological sampling of generically determinate Morrison stegosaurs would allow these proposals to be tested in more depth.

Large body size has been suggested as an adaptation to seasonally arid climatic conditions (Engelmann et al., 2004). Experimental studies of extant megaherbivores demonstrate that as body mass increases, the energy required to maintain physiological life processes increases with increasing body mass (M) according to the relationship $M^{0.75}$ (Engelmann et al., 2004, and references therein). Thus, the higher the body mass, the lower the daily food intake required as a percentage of body mass. As a consequence, larger-bodied taxa are able to make use of poorer quality forage than their small-bodied counterparts. Furthermore, large-bodied animals are able to travel larger distances to move between widely-spaced resources (Engelmann et al., 2004). Under this scenario, size differences between the two genera of stegosaurs found in the Morrison Formation could be related to ecological partitioning, with the larger genus occupying more arid environments than the smaller genus. However, this generalized hypothesis cannot be tested until stratigraphic correlations between the Morrison Formation in Montana, the Bighorn Basin of Wyoming, Utah, and Colorado demonstrate that the two genera were contemporaneous.

ACKNOWLEDGMENTS

LITERATURE CITED

Amprino, R. 1947. La structure du tissu osseux envisagée comme expression de différences dans la vitesse de l'accroissement. Archives de biologie 58:317–330.

Carpenter, K. 2010. Species concepts in North American stegosaurs. Swiss Journal of Geosciences 103:155–162.

Carpenter, K., and P. M. Galton. 2001. Othniel Charles Marsh and the myth of the eight-spiked *Stegosaurus*; pp. 76–102 in K. Carpenter (ed.), The Armored Dinosaurs. Indiana University Press, Bloomington, Indiana.

Carpenter, K., C. A. Miles, and K. Cloward. 2001. New primitive stegosaur from the Morrison Formation, Wyoming. pp. 55–75 in K. Carpenter (ed.), The Armored Dinosaurs. Indiana University Press, Bloomington, Indiana.

Castanet, J., H. Francillon-Vieillot, F. J. Meunier, and A. de Ricqlès. 1992. Bone and individual aging. pp. 245–283 in B. K. Hall (ed.), Bone. Volume 7: Bone Growth–B. CRC Press, London.

Cooley, J. T., and J. G. Schmitt. 1998. An anastomosed fluvial system in the Morrison Formation (Upper Jurassic) of southwest Montana. Modern Geology 22:171–208.

Cope, E. D. 1878. A new genus of Dinosauria from Colorado. The American Naturalist 12:188.

.

Dong, Z.-M. 1973. [Dinosaurs from Wuerho.] Institute of Paleontology and Paleoanthropology Memoir 11:45–52. [Chinese]

Engelmann, G. F., D. J. Chure, and A. R. Fiorillo. 2004. The implications of dry climate for the paleoecology of the fauna of the Upper Jurassic Morrison Formation. Sedimentary Geology 167:297–308.

Francillon-Vieillot, H., V. de Buffrénil, J. Castanet, J. Géraudie, F. J. Meunier, J. Y. Sire, L. Zylberberg, and de Ricqlès, A. 1990. Microstructure and mineralization of vertebrate skeletal tissues. pp. 175–234 in J. G. Carter (ed.), Skeletal Biomineralization: Patterns, Processes and Evolutionary Trends. American Geophysical Union, Washington, D. C.Galton, P. M. 1982. The postcranial anatomy of stegosaurian dinosaur *Kentrosaurus*

from the Upper Jurassic of Tanzania, East Africa. Geologica et Paleontologica 15:139–160

Galton, P. M. 1985. British plated dinosaurs (Ornithischia, Stegosauridae). Journal of Vertebrate Paleontology 5:211–254.

Galton, P. M. 1988. Skull bones and endocranial casts of stegosaurian dinosaur *Kentrosaurus* Hennig, 1915 from Upper Jurassic of Tanzania, East Africa. Geologica et Palaeontologica 22:123–143.

Galton, P. M., and K. Carpenter. 2016. The plated dinosaur *Stegosaurus longispinus* Gilmore, 1914 (Dinosauria: Ornithischia; Upper Jurassic, western USA), type species of *Alcovasaurus* n. gen. Neues Jahrbuch für Geologie und Paläontologie – Abhandlungen 279:185–208.

Gilmore, C. W. 1914. Osteology of the armored Dinosauria in the United States National Museum, with special reference to the genus *Stegosaurus*. United States National Museum Bulletin 89:1–143.

Hayashi, S., K. Carpenter, and D. Suzuki. 2009. Different growth patterns between the skeleton and osteoderms of *Stegosaurus* (Ornithischia: Thyreophora). Journal of Vertebrate Paleontology 29:123–131.

Horner, J. R., and K. Padian. 2004. Age and growth dynamics of *Tyrannosaurus rex*. Proceedings of the Royal Society of London B: Biological Sciences 271:1875–1880.

Horner, J. R., A. de Ricqles, and K. Padian. 1999. Variation in dinosaur skeletochronology indicators: implications for age assessment and physiology. Paleobiology 25:295–304.

Huttenlocker, A. K., H. N. Woodward, and B. K. Hall. 2013. The biology of bone. pp. 13–34 in K.

Padian and E. T. Lamm (eds), Bone Histology of Fossil Tetrapods: Advancing Methods,

Analysis, and Interpretation. University of California Press, Berkeley.ICZN. 2013. Opinion

2320: *Stegosaurus* Marsh, 1877 (Dinosauria, Ornithischia): type species replaced with

Stegosaurus stenops Marsh, 1887. Bulletin of Zoological Nomenclature 70:129–130.

Maidment, S. C. R., and P. M. Barrett. 2012. Does morphological convergence imply functional

similarity? A test using the evolution of quadrupedalism in ornithischian dinosaurs.

Proceedings of the Royal Society of London B: Biological Sciences 279:3765–3771.

Maidment, S. C. R., C. Brassey, and P. M. Barrett. 2015. The postcranial skeleton of an

exceptionally complete individual of the plated dinosaur *Stegosaurus stenops*

(Dinosauria: Thyreophora) from the Upper Jurassic Morrison Formation of Wyoming,

U.S.A. PLoS One 10(10):e0138352.

Maidment, S. C. R., D. B. Norman, P. M. Barrett, and P. Upchurch. 2008. Systematics and

phylogeny of Stegosauria (Dinosauria: Ornithischia). Journal of Systematic Palaeontology

6:364–407.

Marsh, O. C. 1877. A new order of extinct reptilia (Stegosauria) from the Jurassic of the Rocky

Mountains. American Journal of Science, third series 14:34–35.

Marsh, O. C. 1880. Principal characters of American Jurassic dinosaurs. Part III. American

Journal of Science, third series 19:253–259.

Marsh, O. C. 1881. Principal characters of American Jurassic dinosaurs: Part V. American Journal

of Science, third series 21:417–423.

Nopcsa, F. 1915. Die Dinosaurier der Seibenbürgischen Landesteile Ungarns. Mitteilungen aus

dem Jahrbuche der Kniglich Ungarischen Geologischen Reichsanstalt 23:1–26.

Norman, D. B. 1984. A systematic reappraisal of the reptile order Ornithischia; pp. 157–162 in

W.-E. Reif, and F. Westphal (eds.), Third Symposium on Mesozoic Terrestrial Ecosystems,

Short Papers. Attempto Verlag, Tübingen.

Owen, R. 1842. Report on British fossil reptiles. Reports of the British Association for the

Advancement of Science 11:60–204.

Padian, K., and E. T. Lamm. 2013. Bone histology of fossil tetrapods: advancing methods,

analysis, and interpretation. University of California Press, Berkeley, 285 pp.

Raven, T. J., and S. C. R. Maidment. In press. A new phylogeny of Stegosauria (Dinosauria,

Ornithischia. *Palaeontology*. DOI: 10.1111/pala12291.

Redelstorff, R., and P. M. Sander. 2009. Long and girdle bone histology of *Stegosaurus*:

implications for growth and life history. Journal of Vertebrate Paleontology 29:1087–

1099.

Ricqlès, A. de, F. J. Meunier, J. Castanet, and H. Francillon-Vieillot. 1991. Comparative microstructure of

bone. Bone 3:1-78.Sander, P. M. and N. Klein. 2005. Developmental plasticity in the life

history of a prosauropod dinosaur. Science 310:1800–1802.

Seeley, H. G. 1887. On the classification of the fossil animals commonly named Dinosauria.

Proceedings of the Royal Society of London 43:165–171.

Sereno, P. C., and Z.-M. Dong. 1992. The skull of the basal stegosaur *Huayangosaurus taibaii*

and a cladistics diagnosis of Stegosauria. Journal of Vertebrate Paleontology 12:318–

343.

Whitlock, J. A., and J. D. Harris. 2010. The dentary of *Suuwassea emilieae* (Sauropoda: Diplodocoidea). Journal of Vertebrate Paleontology 30:1637–1641.

Wilson, J. A. 1999. A nomenclature for vertebral laminae in sauropods and other saurischian dinosaurs. Journal of Vertebrate Paleontology 19:639–653.

Woodruff, D. C., and D. W. Fowler. 2012. Ontogenetic influence on neural spine bifurcation in Diplodocoidea (Dinosauria: Sauropoda): a critical phylogenetic character. Journal of Morphology 273:754–764.

Woodward, H. N., and A. H. Lee. 2013. Skeletochronology. pp. 195–216 in K. Padian and E. T. Lamm (eds), Bone Histology of Fossil Tetrapods: Advancing Methods, Analysis, and Interpretation. University of California Press, Berkeley.Woodward, H. N., E. A. F. Fowler, J. O. Farlow, and J. R. Horner. 2015. *Maiasaura*, a model organism for extinct vertebrate population biology: a large sample statistical assessment of growth dynamics and survivorship. Paleobiology 41:503–527.

Woodward, H. N., J. R. Horner, and J. O. Farlow. 2014. Quantification of intraskeletal histovariability in *Alligator mississippiensis* and implications for vertebrate osteohistology. PeerJ 2:e422.

Zhou, S. 1984. [The Middle Jurassic dinosaurian fauna from Dashanpu, Zigong, Sichuan, Volume 2: stegosaurs]. Sichuan Scientific and Technological Publishing House, Sichuan, 52 pp. [Chinese with English summary].

FIGURE CAPTIONS

FIGURE 1. Location of the O'Hair quarry, southern Montana [Full page width]

FIGURE 2. Stratigraphy of the O'Hair quarry. Sedimentological log measured through the lower and upper O'Hair quarries. MOR 9728, *Hesperosaurus mjosi*, was found along strike of the main quarries, and the approximate stratigraphic location is shown here. Lack of exposure prevents examination of the Morrison Formation outside of the quarry interval. Grainsize intervals are clay, **c;** silt, **s**; very fine sand, fine sand, medium sand, **ms**; coarse sand, gravel, **g**; not all are labelled for clarity [2/3 page width].
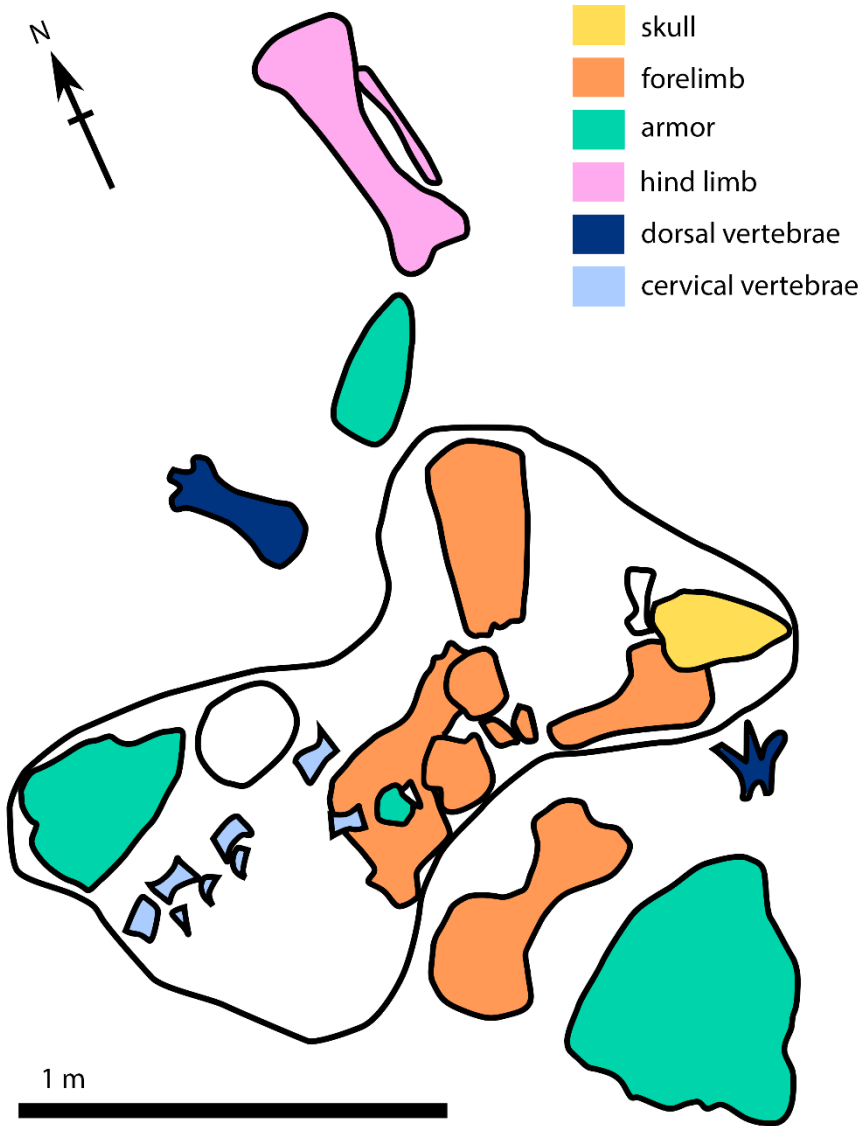
FIGURE 3. Quarry map during excavation of *Hesperosaurus mjosi*, MOR 9728. Unlabelled elements are unknown or not from MOR 9728 [2/3 page width].

FIGURE 4. Skull of MOR 9728, *Hesperosaurus mjosi*, with individual blocks labelled. Scale bar equal to 10 cm [full page width].
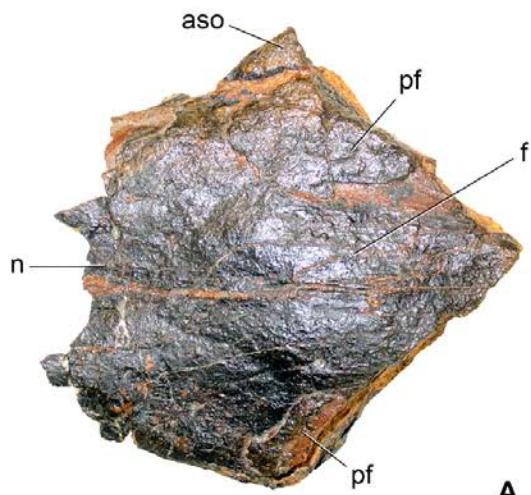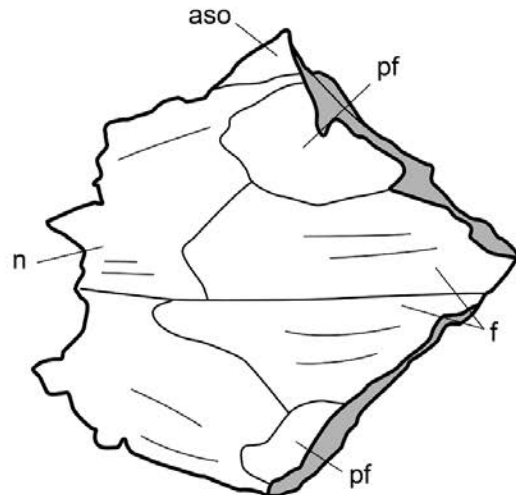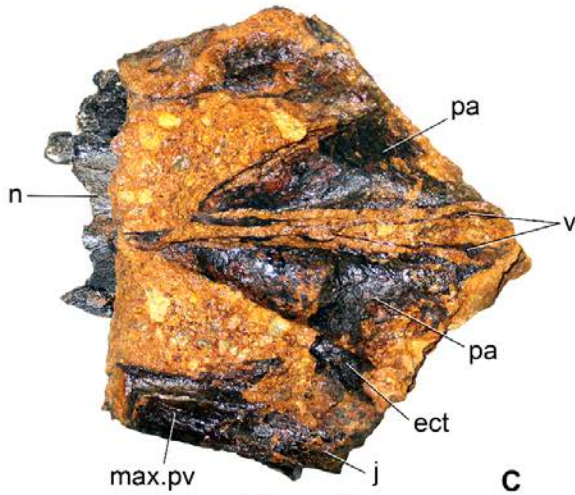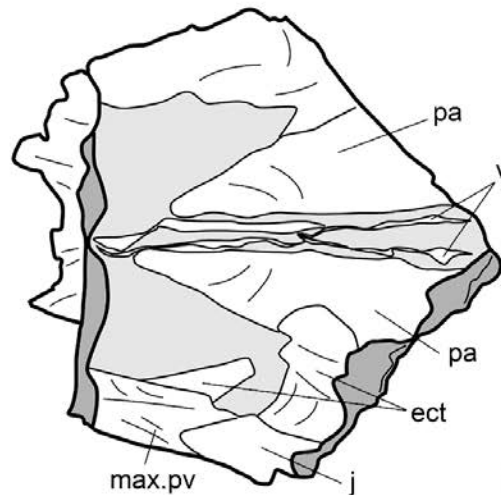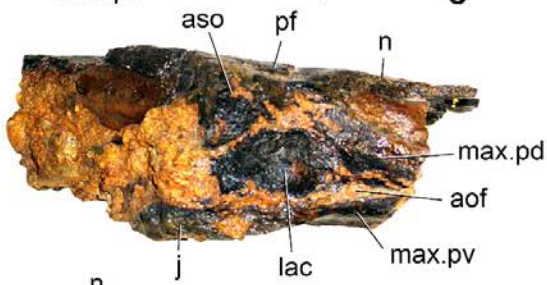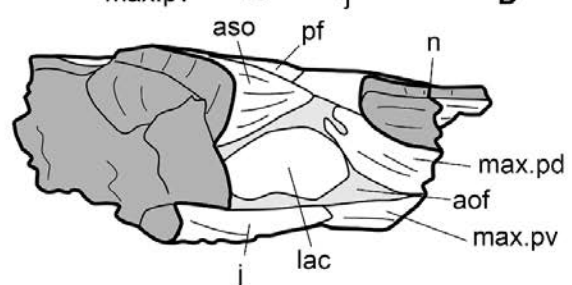
FIGURE 5. MOR 9728, *Hesperosaurus mjosi*, skull block 2 in **A, B**, dorsal, **C, D**, ventral, **E, F**, right lateral, **G**, left lateral views. Anterior is to the left in **A-D** and **G**, and to the right in **C-D**.

Abbreviations: aof, antorbital fossa; **aso**, anterior supraorbital; **ect**, ectopterygoid; **f**, frontal; **j**, jugal; **lac**, lacrimal; **max.pd**, posterodorsal process of the maxilla; **max.pv**, posteroventral process of the maxilla; **n**, nasal; **pa**, palatine; **pf**, prefrontal; **v**, vomer. Scale bar equals 2 cm. [Full page width].
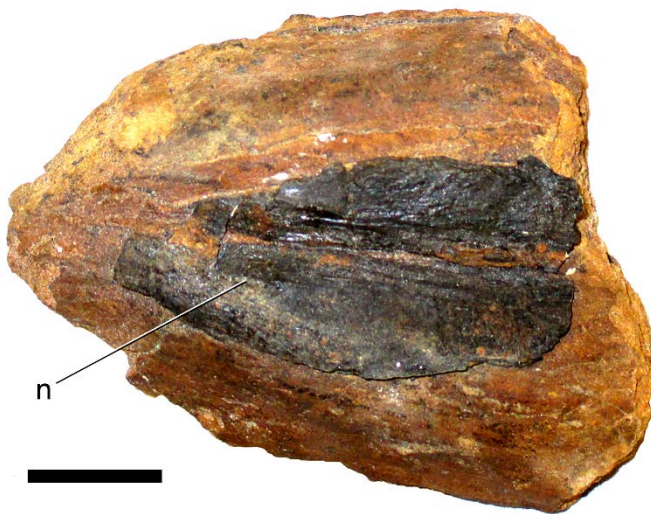
FIGURE 6. MOR 9728, *Hesperosaurus mjosi*, skull block 1, showing nasals, **n**, in dorsal view. [Column width].
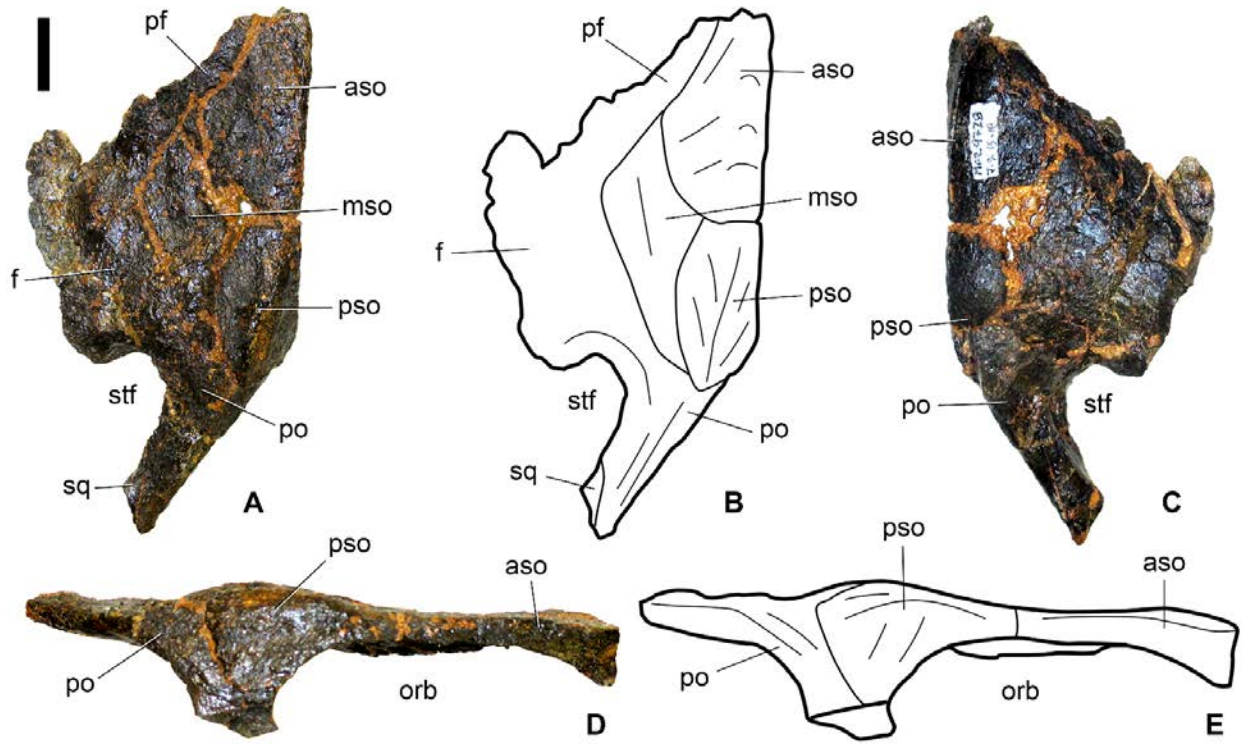
FIGURE 7. MOR 9728, *Hesperosaurus mjosi*, skull block 4 in **A, B**, dorsal, **C**, ventral and **D, E**, right lateral views. Anterior is to the top of the page for **A-C**, and to the right for **D** and **E**.

Abbreviations: aso, anterior supraorbital; **f**, frontal; **mso**, median supraorbital; **orb**, orbit; **pf**, prefrontal; **po**, postorbital; **pso**, posterior supraorbital; **stf**, supratemporal fenestra. Scale bar equals 2 cm. [Full page width].
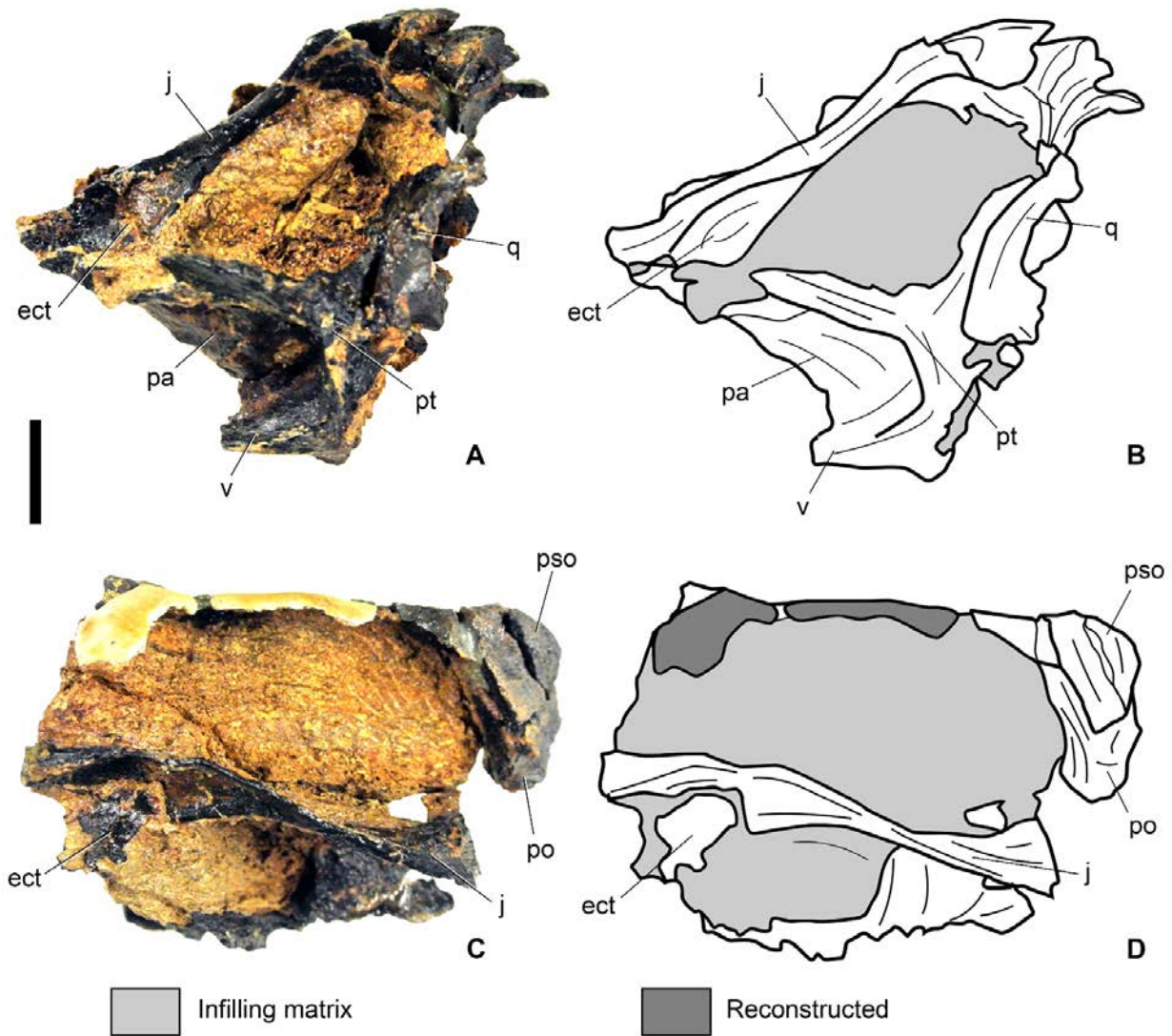
FIGURE 8. MOR 9728, *Hesperosaurus mjosi*, skull block 3 in **A, B**, ventral and **C, D**, left lateral views. Anterior is to the left in **A-D. Abbreviations: ect**, ectopterygoid; **j**, jugal; **pa**, palatine; **po**, postorbital; **pso**, posterior supraorbital; **pt**, pterygoid; **v**, vomer. Scale bar equals 2 cm. [Full page width].
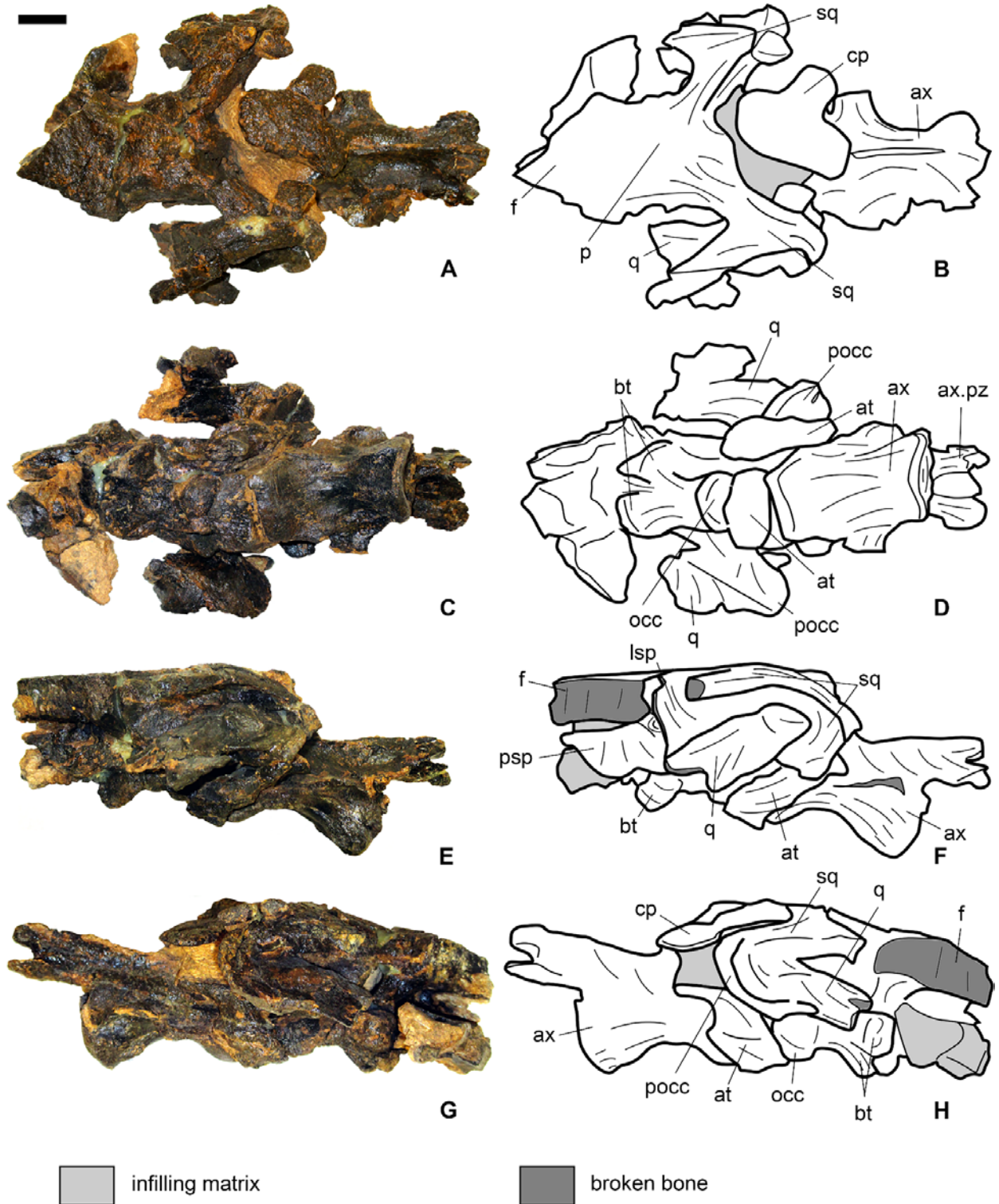
FIGURE 9. MOR 9728, *Hesperosaurus mjosi*, skull block 5 in **A, B**, dorsal, **C, D**, ventral, **E, F**, left lateral and **G, H**, right lateral views. Anterior is to the left in **A-F** and to the right in **G-H**.

Abbreviations: at, atlas; **ax**, axis; **ax.pz**, axis postzygapophyses; **bt**, basal tubera; **cp**, cervical dermal plate?; **f**, frontal; **lsp**, laterosphenoid; **occ**, occipital condyle; **p**, parietal; **pocc**, paroccipital process; **psp**, parasphenoid; **q**, quadrate; **sq**, squamosal. Scale bar equals 2 cm. [Full page width].
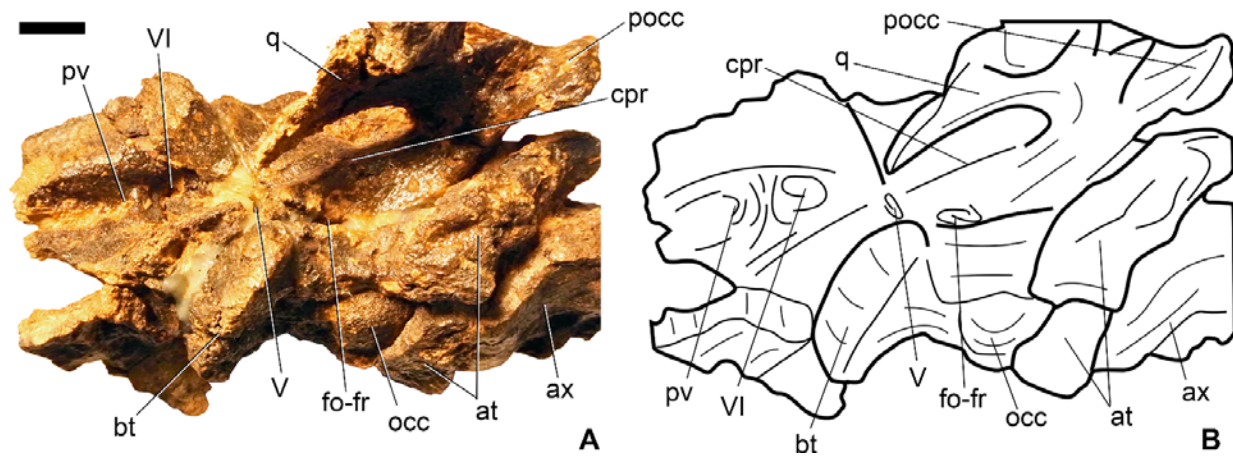
FIGURE 10. MOR 9728, *Hesperosaurus mjosi*, detail of braincase in left lateral oblique view.

Abbreviations: at, atlas; **ax**, axis; **bt**, basal tubera; **cpr**, crista prootica; **fo-fr**, combined fenestra ovalis and fenestra pseudorotunda; **occ**, occipital condyle; **pocc**, paroccipital process; **pv**, foramen for the pituitary vein; **q**, quadrate; **V**, trigeminal foramen; **VI**, abducens foramen. Scale bar equals 2 cm. [Full page width].
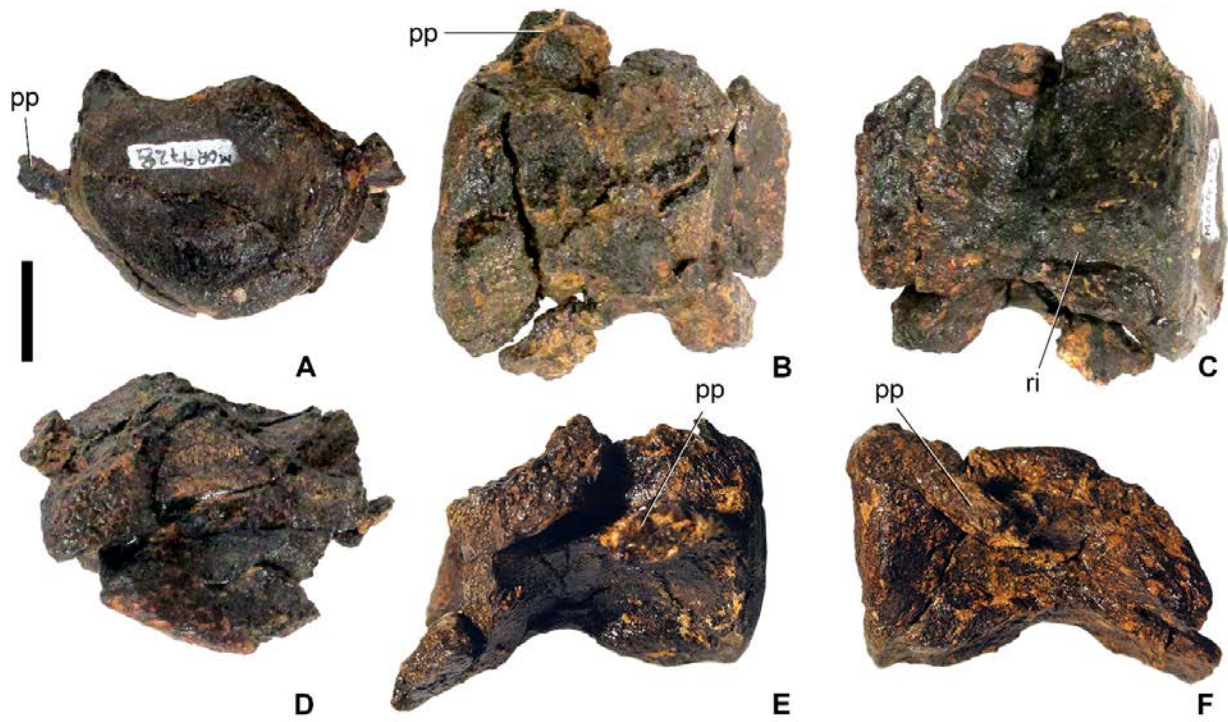
FIGURE 11. MOR 9728, *Hesperosaurus mjosi*, cervical vertebra one in **A**, anterior, **B**, dorsal, **C**, ventral, **D**, posterior, **E**, right lateral and **F**, left lateral view. **Abbreviations: pp**, parapophysis; **ri**, ridge. Scale bar equals 2 cm. [Full page width].
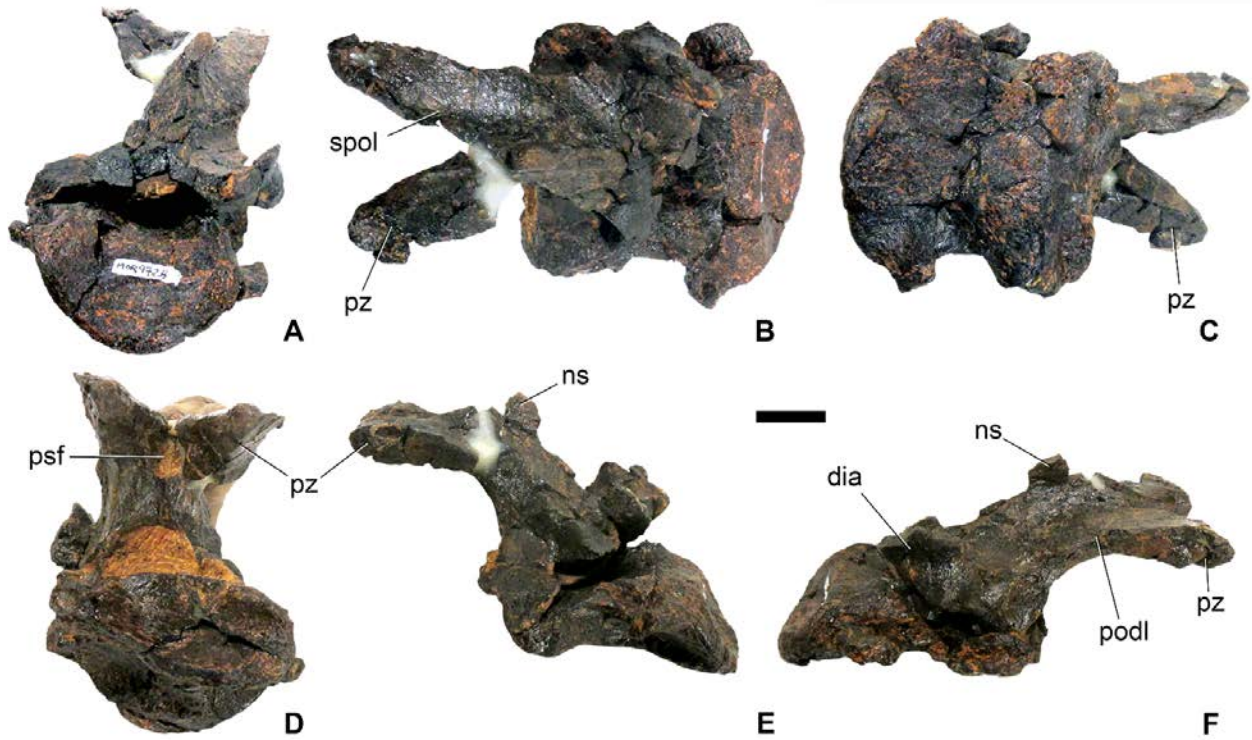
FIGURE 12. MOR 9728, *Hesperosaurus mjosi*, cervical vertebra two **A**, anterior, **B**, dorsal, **C**, ventral, **D**, posterior, **E**, right lateral and **F**, left lateral view. **Abbreviations: dia**, diapophysis; **ns**, neural spine; **podl**, postzygodiapophyseal lamina; **psf**, postspinal fossa; **pz**, postzygapophysis; **spol**, spinopostzygopophyseal lamina. Scale bar equals 2 cm. [Full page width].
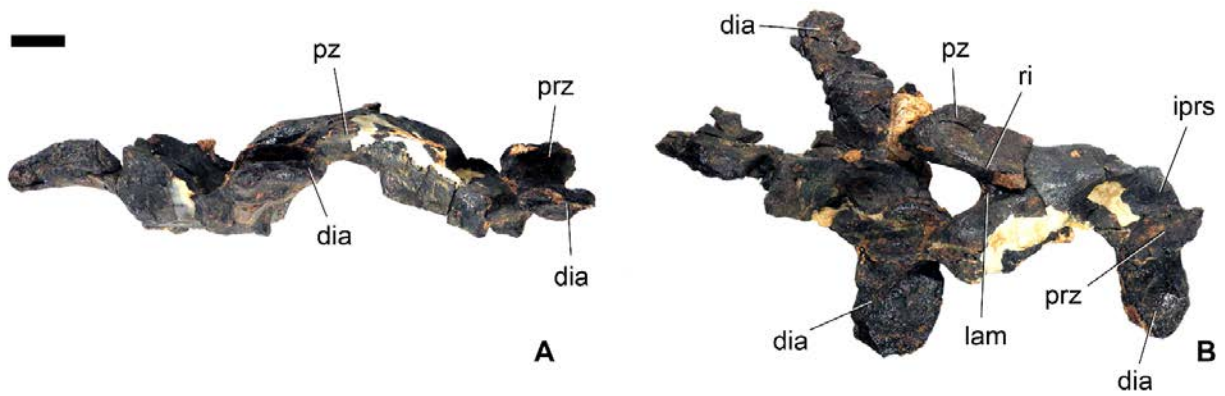
FIGURE 13. MOR 9728, *Hesperosaurus mjosi*, articulated cervical neural arches in **A,** right lateral and **B,** dorsal views. **Abbreviations: dia**, diapophysis; **iprs**, intraprezygapophyseal shelf; **lam**,

lamina; **prz**, prezygapophysis; **pz**, postzygapophysis; **ri**, ridge. Scale bar equals 2 cm. [Full page width].
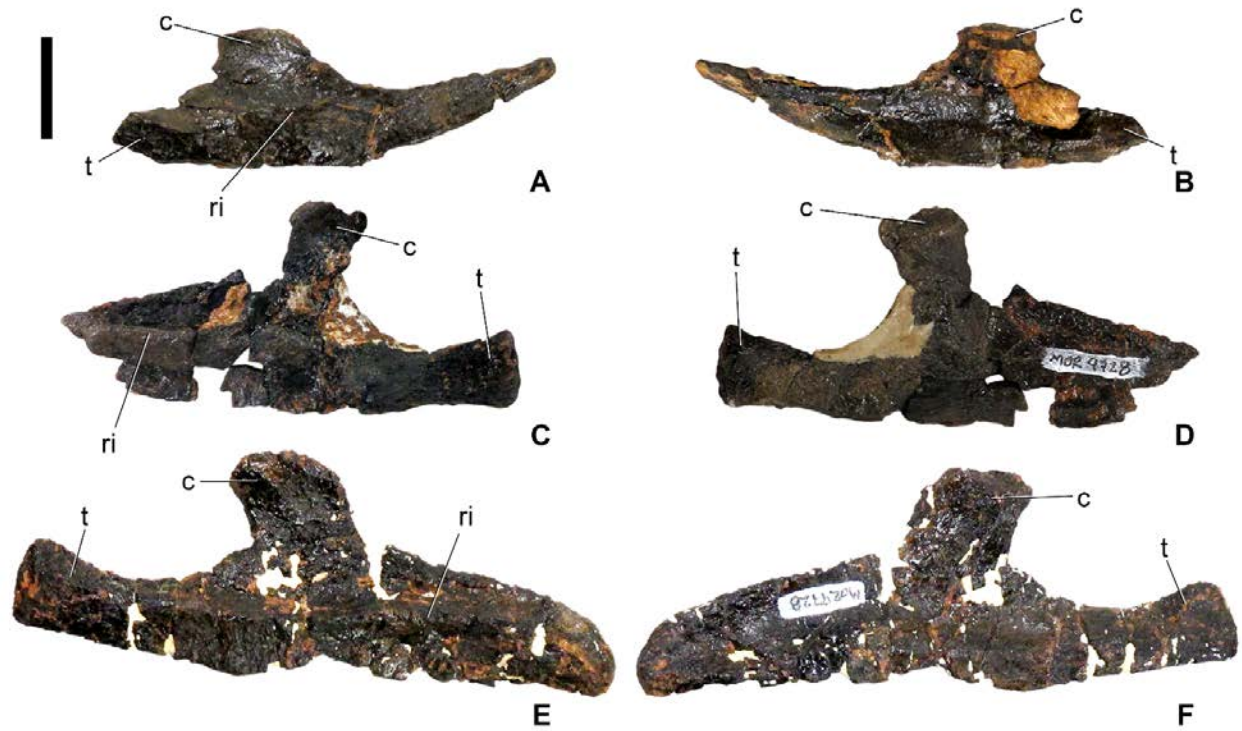
FIGURE 14. MOR 9728, *Hesperosaurus mjosi*, cervical ribs in **A, C, E**, lateral and **B, D, F**, medial views. **Abbreviations: c**, capitulum; **ri**, ridge; **t**, tuberculum. Scale bar equals 2 cm. [Full page width].
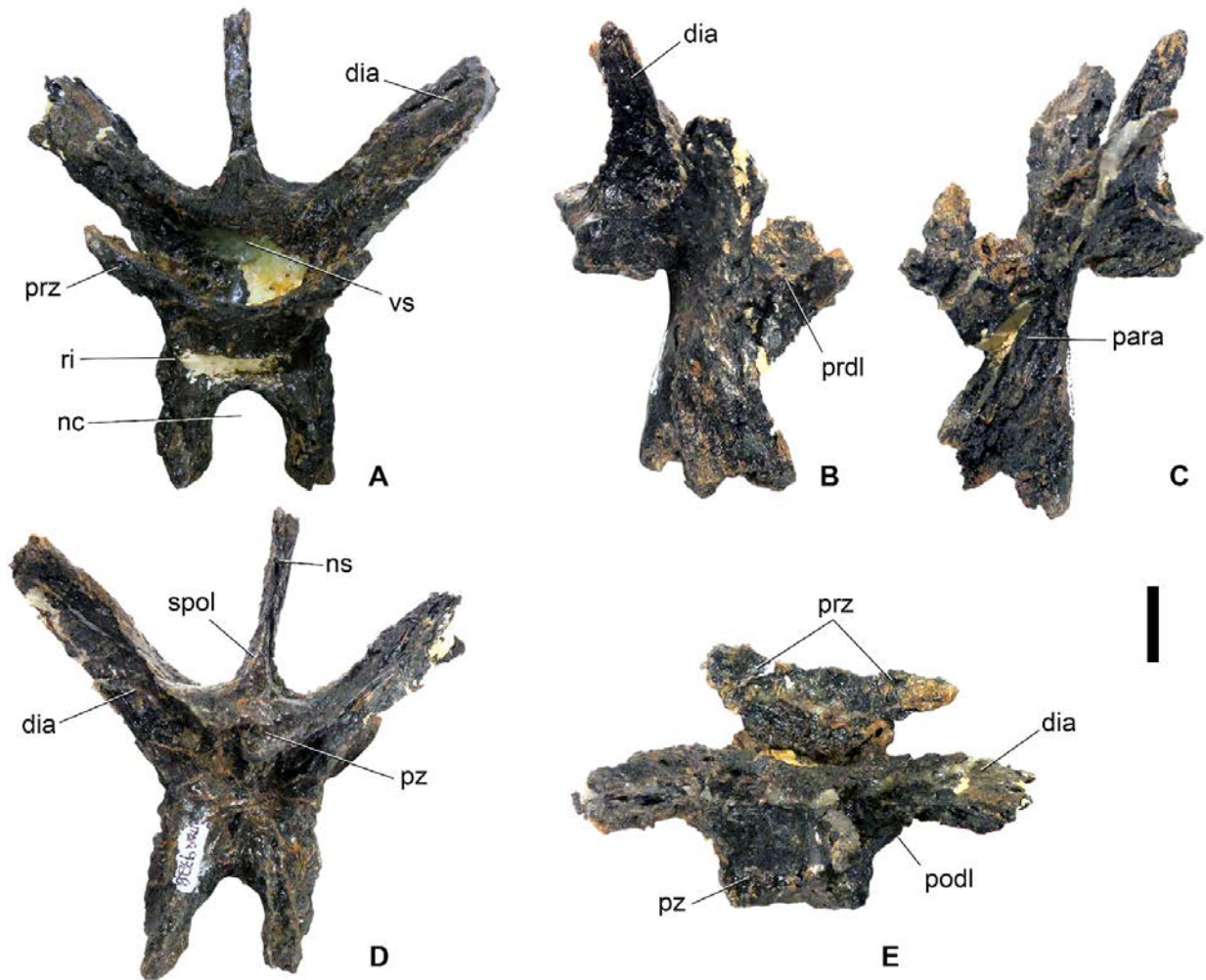
FIGURE 15. MOR 9728, *Hesperosaurus mjosi*, dorsal neural arch in **A**, anterior, **B**, right lateral, **C**, left lateral, **D**, posterior and **E**, dorsal views. **Abbreviations: dia**, diapophysis; **nc**, neural canal; **ns**, neural spine; **para**, parapophysis; **podl**, postzygodiapophyseal lamina; **prdl**, prezygodiapophyseal lamina; **prz**, prezygapophysis; **pz**, postzygapophysis; **ri**, ridge; **spol**, spinopostzygapophyseal lamina; **vs**, vertical sheet. Scale bar equals 2 cm. [Full page width].
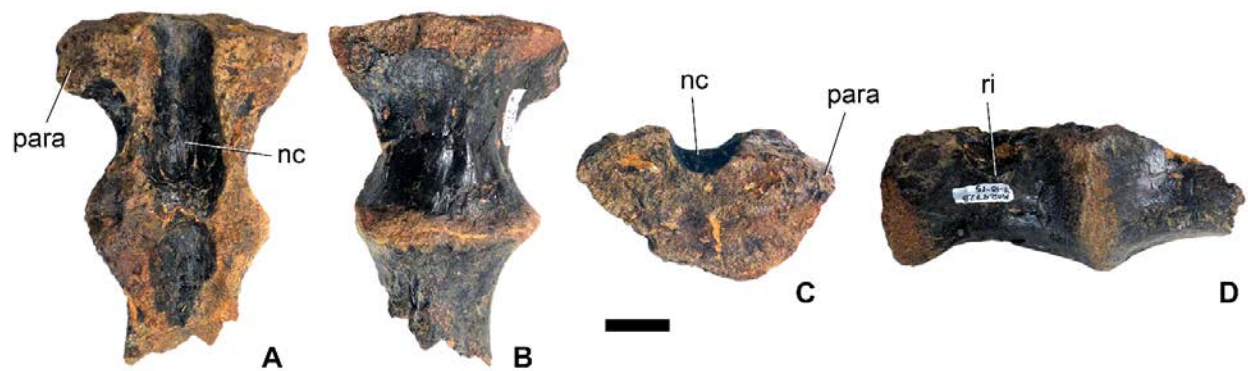
FIGURE 16. MOR 9728, *Hesperosaurus mjosi*, sacrum in **A**, dorsal, **B**, ventral, **C**, anterior and **D,** left lateral views. **Abbreviations: nc**, neural canal; **para**, parapophyses; **ri**, ridge. Scale bar equals 2 cm. [Full page width].
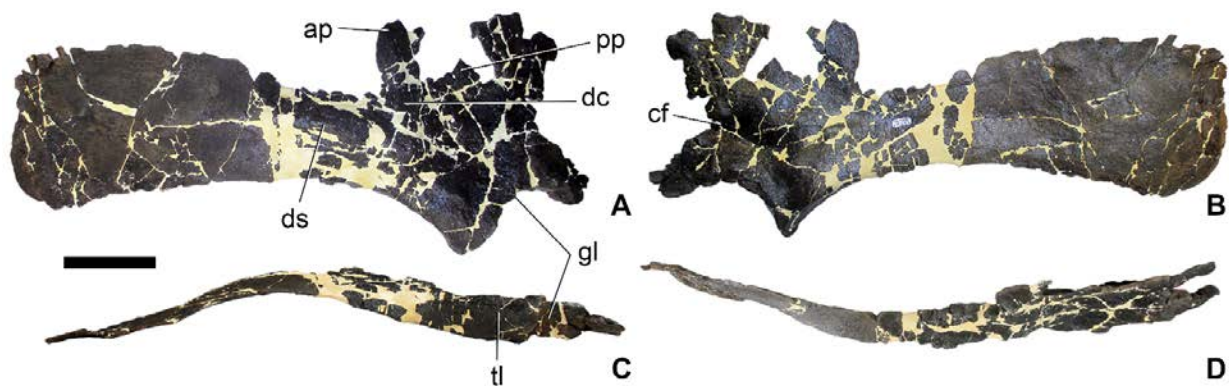
FIGURE 17. MOR 9728, *Hesperosaurus mjosi*, right scapulocoracoid in **A**, lateral, **B**, medial, **C**, ventral and **D**, dorsal views. **Abbreviations: ap**, acromial process; **cf**, coracoid foramen; **dc**, *deltoideus clavicularis* ridge; **ds**, *deltoideus scapularis* ridge; **gl**, glenoid; **pp**, proximal plate; **tl**, muscle scar for *triceps longus*. Scale bar equals 10 cm. [Full page width].
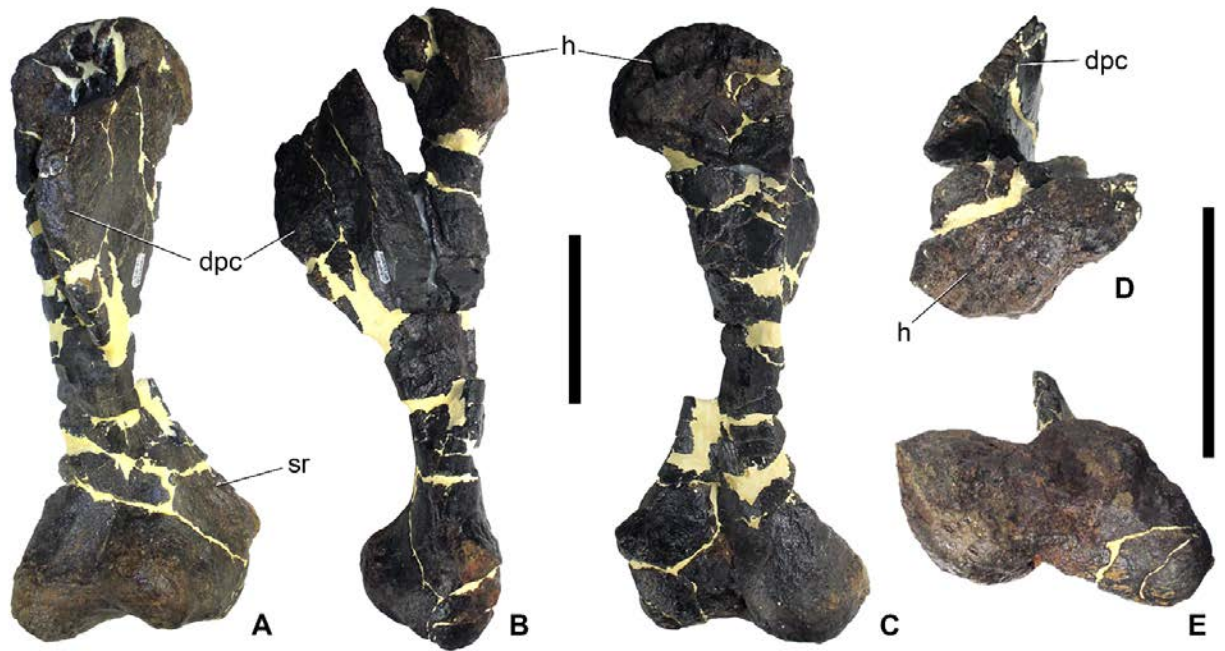
FIGURE 18. MOR 9728, *Hesperosaurus mjosi*, left humerus in **A**, anterior, **B**, lateral, **C**, posterior, **D**, dorsal and **E**, ventral views. **Abbreviations: dpc**, deltopectoral crest; **h**, head; **sr**, supinator ridge. Scale bars equals 10 cm. [Full page width].
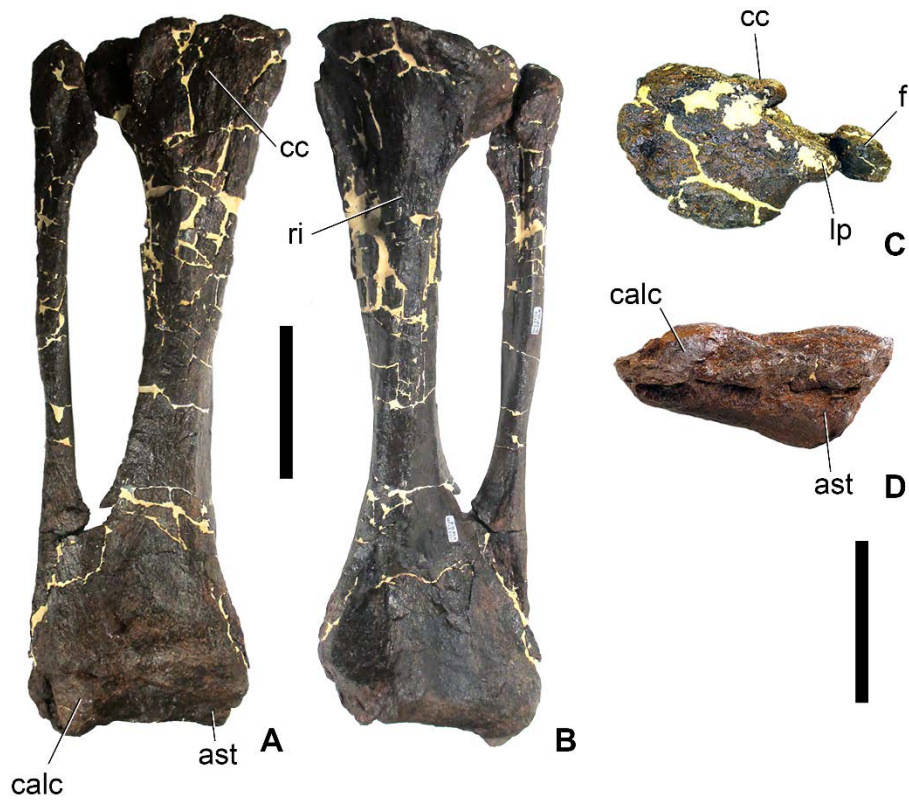
FIGURE 19. MOR 9728, *Hesperosaurus mjosi*, right tibia, fibula, astragalus and calcaneum in **A**, anterior, **B**, posterior, **C**, dorsal and **D**, ventral views. **Abbreviations: ast**, astragalus; **calc**, calcaneum; **cc**, cnemial crest; **f**, fibula; **lp**, lateral process. Scale bars equals 10 cm. [2/3 page width].
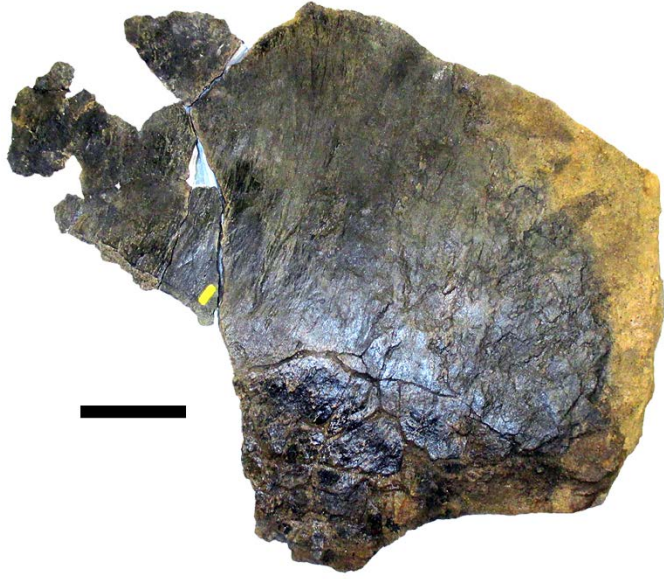
FIGURE 20. MOR 9728, *Hesperosaurus mjosi*, dorsal plate in medial/lateral view. Scale bar equals 10 cm. [Column width].

A.

B.

Outer cortex with decreasing generations of secondary osteons (max. of 2)with more LAGs evident in the outermost region

Highly remodeled zone (3-4 generations of secondary osteons) with a few LAGs present

Medullary cavity

D.

Decreasing vascularity

SMA0092

E.

Decreasing vascularity

VFSMA001

C.

Decreasing vascularity
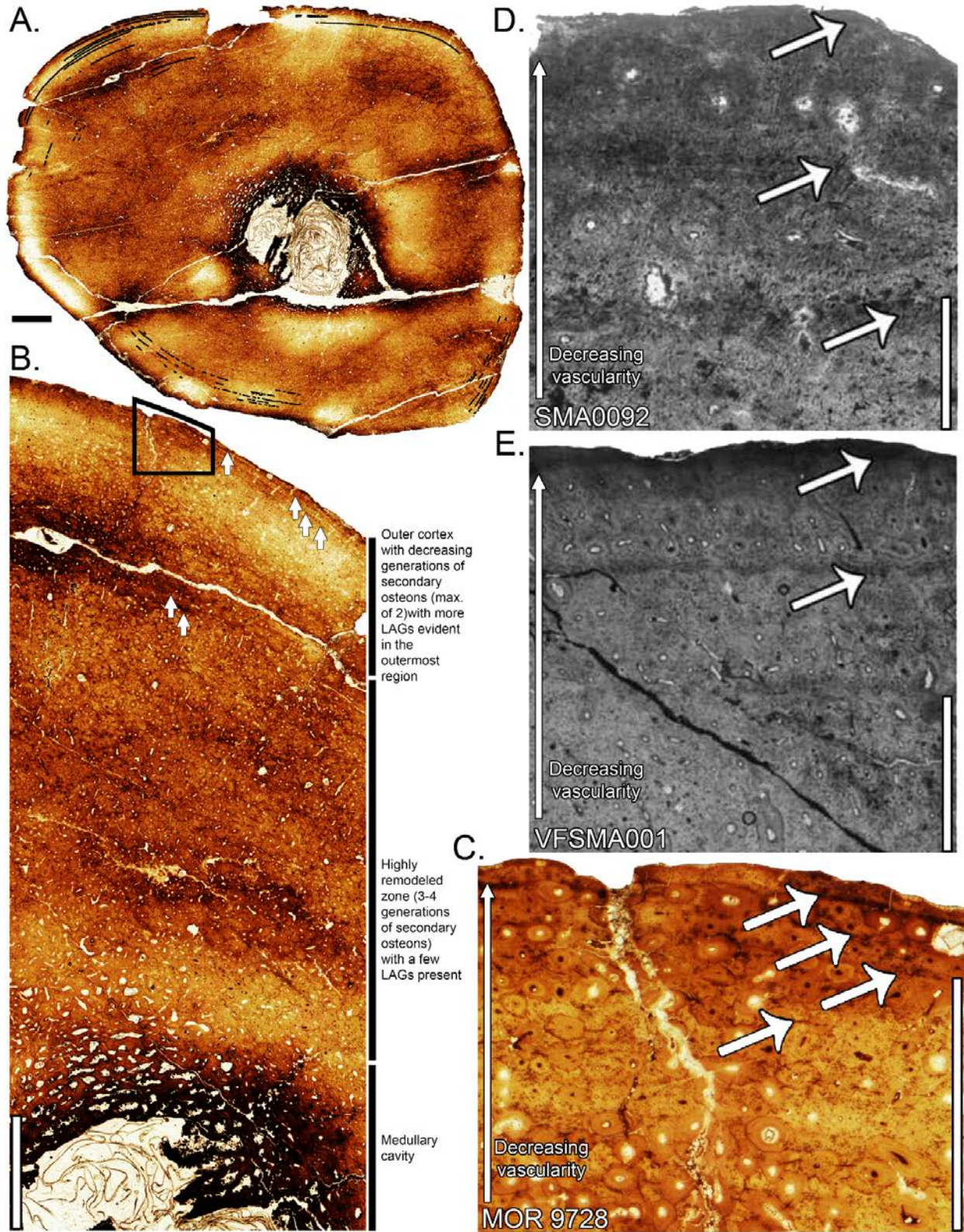
MOR 9728

FIGURE 21. Histologic analysis of the left tibia of MOR 9728, *Hesperosaurus mjosi*. **A,**the entire

tibia transverse section; black lines highlight Lines of Arrested Growth (LAGs).. **B,** magnified

section showing the medullary cavity to the outermost cortex and highlighting the

circumferential decrease in remodeling, and LAGs marked with white arrows. **C,** further

magnification of the area in the black box in **B.** The outermost cortex shows zones of differing

vascularity, and four LAGs denoted with large white arrows. **D, E,** comparable sections from *S.*

mjosi specimens SMA0092 and VFSMA001 (from Redelstorff and Sander, 2009, reproduced by

permission from the Society of Vertebrate Paleontology (www.vertpaleo.org)). Scale bar equals

1 cm in **A** and **B**, 1.5 mm in **C**, 0.25 mm in **D**, and 1 mm in **E**. [Full page width].
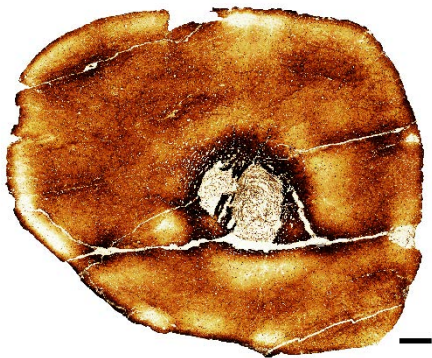
SUPPLEMENTARY INFORMATION FIGURE 1. Transverse histologic thin section of the left tibia of

MOR 9728, *Hesperosaurus mjosi*. Scale bar in part A equals 1 cm.
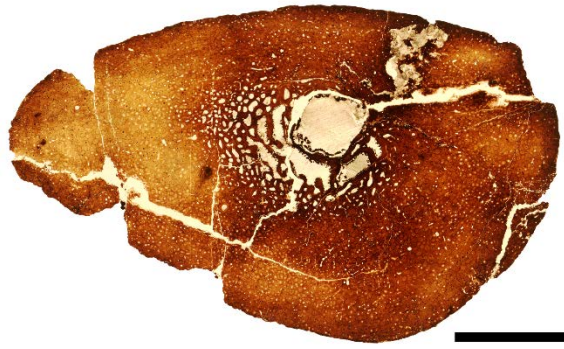
SUPPLEMENTARY INFORMATION FIGURE 2. Transverse histologic thin section of the left fibula

of MOR 9728, *Hesperosaurus mjosi*. Scale bar equals 1 cm.